RIVER METABOLISM AND CARBON CYCLING IN A HEAVILY IMPACTED AGRICULTURAL WATERSHED

ILYANNA JANVIER

Bachelor of Science, University of Lethbridge, 2022

A thesis submitted in partial fulfilment of the requirements for the degree of

MASTER OF SCIENCE
in
BIOLOGICAL SCIENCES

Department of Biological Sciences
University of Lethbridge
Lethbridge, Alberta, Canada

EXPLORING RIVER METABOLISM AND CARBON CYCLING IN A HEAVILY IMPACTED AGRICULTURAL WATERSHED

Ilyanna Janvier

Date of Defence: 18th December 2024

Dr. Matthew J Bogard Thesis Supervisor	Associate Professor	Ph.D.
Dr. Cameron P Goater Thesis Examination Committee member	Professor	Ph.D.
Dr. Erin R Hotchkiss Thesis Examination Committee member	Associate Professor	Ph.D.
Theresa Burg Chair, Thesis Examination Committee member	Professor	Ph.D.

ABSTRACT

Rivers support people in many ways, including for agriculture and irrigation, drinking water, and recreational and cultural uses. Streams and rivers also play an important role in the global carbon (C) cycle as they not only transport C and nutrients to the ocean, but they also store, emit, and transform different sources of C. Consequently, rivers contribute large quantities of carbon dioxide (CO_2) to the atmosphere. Human activities can modify food web metabolism and the cycling of C in rivers in complex ways that are hard to predict. For streams and rivers in southern Alberta, one of Canada's most heavily impacted agricultural landscapes, riverine metabolism and C cycling are not well quantified. Here, I explore these issues in the Little Bow River (LBR) and Mosquito Creek (MCR). I used a combination of methods including both low and high frequency measurements to calculate CO_2 flux, microbial incubations to measure C consumption, and whole-river metabolism. My research revealed that concentrations of CO_2 were low compared to the global average, and as a result, emissions were also generally low in the river network. I found that modelled rates of metabolism in the river network, on average, were higher for gross primary production (GPP) but lower for ecosystem respiration (ER) than median rates reported for global rivers, and the network was generally on the low side for metabolic rates compared to streams in other agricultural regions. I document a shift in C cycling patterns from headwaters to the lower river, by showing increased coupling of GPP and ER, decreased bioavailability of DOC, and ultimately, elevated pH and lower CO_2 emissions downstream. Human controls on flow regimes appeared to be the driving factor for differences between sites throughout the network. My research presents new network-scale patterns of river C cycling in drought-stressed agricultural landscapes.

ACKNOWLEDGEMENTS

To begin, I want to thank my supervisor Dr. Matthew Bogard, for not only inspiring me to pursue a master's degree and my love for this discipline, but for the immense support, reassurance, and kindness to help me push forward. I am beyond thankful for his support through not only my academic journey but personal development. I am also grateful for my committee members Dr. Cam Goater and Erin Hotchkiss for their guidance and feedback on my research. I can't thank all of the wonderful members of the Bogard lab enough, especially Molly, Jackie, Laura, and Mariya, for all the help in the field, lab work, coding, and the emotional support. Major appreciation for the friends I have made through the program, Amanda, Jemma, and Rayan, as you three have kept me sane and provided endless laughs as we struggle together. Thank you to my childhood best friend Janelle, for your kindness, willingness to listen, and overwhelming support and confidence in me. I also can't express how grateful I am for my partner Brett, who has been by my side to support, encourage, and motivate me through challenging times.

Finally, I want to express my heartfelt gratitude to my friends and family, especially my parents and little sisters, as your unwavering support has been instrumental in my success and in helping me reach my goals. You have pushed me to go above and beyond of what I thought I was capable of and provided me with endless love.

TABLE OF CONTENTS

LIST OF TABLES

LIST OF FIGURES

LIST OF ABBREVIATIONS

ANOVA	Analysis of variance
BDOC	Biodegradable dissolved organic carbon
C	Carbon
CH_4	Methane
Chl *a*	Chlorophyll a
CO_2	Carbon dioxide
CO_3^{-2}	Carbonate
DIC	Dissolved inorganic carbon
DOC	Dissolved organic carbon
DOM	Dissolved organic matter
F_{CO2}	Flux of carbon dioxide to atmosphere
GHG	Greenhouse gas
HCO_3^-	Bicarbonate
HF	High frequency
IC	Inorganic carbon
LBCAN	Little Bow River canal
LBCAR	Little Bow River at Carmangay
LBUP	Little Bow River above frank lake drain
LB533	Little Bow River at Highway 533
MCR	Mosquito Creek
MCRDIV	Mosquito Creek diversion
TVRD	Twinn Valley Reservoir downstream
TVR	Twin Valley Reservoir
OC	Organic carbon
OM	Organic matter
pCO_2	CO_2 partial pressure
POC	Particulate organic carbon

CHAPTER 1. INTRODUCTION

1.1 Background

1.1.1. The Global Carbon Cycle

Carbon (C) is the building block of life on Earth and is the fourth most abundant element in the universe (Teyssier et al., 2004). The C cycle regulates Earth's climate through the production and consumption of important greenhouse gases, including carbon dioxide (CO_2) and methane (CH_4), which trap heat that is then returned to Earth's surface (Schlesinger and Bernhardt 2020). The global C cycle involves fluxes through various pools (Fig. 1). The dominant pools include the oceans (3.8×10^{19} g C), terrestrial landscape (soils and vegetation; 3.0×10^{18} g C), and atmosphere (8.6×10^{17} g C) (Fig. 1). Atmospheric CO_2 can be taken up by photosynthesizing plants (1.2×10^{17} g C yr^{-1}; Fig. 1) and bacteria to create organic matter (OM). This OM is then transferred through food webs and ultimately decomposed and respired by terrestrial and aquatic organisms that release CO_2 at rates of 6.0, 6.0 and 9.0×10^{16} g C yr^{-1} for terrestrial plants and soils and marine habitats, respectively (Fig. 1). The ocean is one of the largest C sinks, as it absorbs CO_2 from the atmosphere at rates of 9.3×10^{16} g C yr^{-1} (Fig. 1) through both biological and abiotic processes (Schlesinger & Bernhardt, 2020). A small fraction of the C in the ocean is sedimented each year (2×10^{14} g C yr^{-1}; Fig. 1). Land-to-ocean export of C is also an important flux in the global C budget and is relatively well-defined (0.8 Pg C yr^{-1}). Human activities have also altered the global C cycle, as fossil fuel burning is mobilizing previously-stored ancient C into the active C cycle (IPCC 2014; Butman et al. 2015). The burning of fossil fuels such as coal, oil, and natural gas is currently transferring C into the atmosphere at rates of 9.9×10^{15} g C yr^{-1}(Fig. 1).

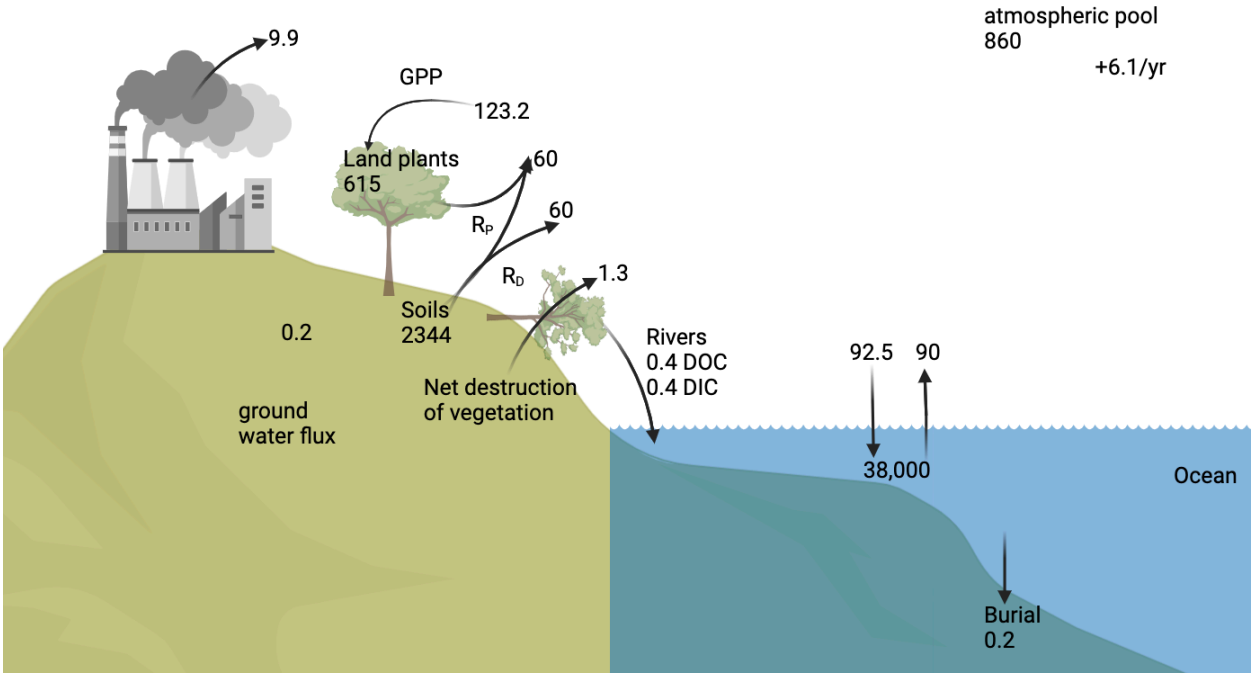

Figure 1. The global carbon cycle with values for 2016. The pools are reported in units of 10^{15} g C and the fluxes as 10^{15} g C yr^{-1}. Revised from Schlesinger and Bernhardt (2020).

1.1.2. Role of Rivers in the Global C Cycle

Inland waters (lakes, rivers, wetlands, reservoirs), once overlooked, actively participate in the global C cycle by intercepting terrestrial C lost from land to aquatic networks. Prior to coastal export, 1.9 to 5.1 Pg yr^{-1} of C lost from land is intercepted by streams, lakes, and reservoirs (collectively, the aquatic network) (Cole et al., 2007, Drake et al., 2018). Processing of terrestrial C in aquatic networks sustains emissions of large quantities of CO_2 and CH_4 to the atmosphere (Cole et al., 2007; Battin et al., 2009; Rocher-Ros et al., 2023) (Fig. 2). Among all inland waters (lakes, rivers, and reservoirs), most emissions of CO_2 (1.8 Pg C yr^{-1}) are derived from rivers and streams (Raymond et al., 2013). Internal production of CO_2 through heterotrophic metabolic pathways in rivers is largely fueled by particulate and dissolved organic carbon (POC and DOC, respectively; Fig. 2) that is fixed on land and transported from terrestrial and wetland riparian habitats into rivers (Duarte & Prairie, 2005; Duarte & Augusti, 1998; Abril et al., 2014). This is an external source of C to aquatic environments, or allochthonous inputs, that derive from litterfall, soils, and other sources from the surrounding terrestrial and riparian floodplain environments (Abril et al., 2014). In addition to metabolic processes, internal production of CO_2 can also be supported through abiotic processes, including photochemical breakdown of organic matter (Lapierre et al., 2013; Cory et al., 2014). Autochthonous C is produced from sources within the river and contributes to the total OC pool (Fig. 2), and it can also be mineralized and released as CO_2 (Kritzberg et al., 2004). The balance of this internally derived versus externally derived CO_2 (and thus the source of emissions) is not static and depends on changes in land cover, connectivity with the land, climate, and terrestrial processing (e.g., Hotchkiss et al., 2015). Therefore, rivers not only act as passive “pipes” that carry C to the oceans but are now recognized as reactors that generate CO_2 internally and modify the chemical composition of the OM pool as it transits through

the network (Cole et al., 2007; Tranvik et al., 2009). The OM fixed on land is consumed by microbes (free and benthic) in rivers and can be modified or replaced by internally derived materials that are chemically distinct (Kellerman et al., 2014). Knowing the source of emitted CO_2 (land derived and exported versus produced in the river itself) is critical to obtaining an accurate global C budget (Hotchkiss et al.,2015; Abril et al. 2014; Battin et al., 2023).

1.1.3. Human Impacts on Riverine C Cycling

Land disturbance and alterations change the biogeochemistry of rivers by adding an additional ~ 1.0 Pg C yr^{-1} to aquatic networks (Regnier et al., 2013). Human activities that enhance catchment weathering (e.g., agriculture and forestry) directly add inorganic carbon (IC) and organic carbon (OC) to aquatic networks (~0.9 Pg), while sewage release adds an additional ~0.1 Pg C yr^{-1} into aquatic networks (Regnier et al., 2013). The form of human-derived C entering river systems can impact ecosystem functioning (Fig. 2). For instance, the addition of particulates may change the extent of light attenuation, which affects photosynthesis and light-dependent reactions (Bauer et al, 2013). In addition, differences in the chemical composition of materials transported to rivers can impact the photochemical and biological reactivity of OC (Bauer et al., 2013), and impact rates of internal CO_2 production (Fig. 2). Land disturbance can also input previously-stored aged soil C into river systems, which stimulates microbial respiration, photodegradation, and enhances CO_2 emissions (Butman et al., 2015) (Fig.2). This mechanism may be of greater importance in smaller watersheds (Butman et al., 2015).

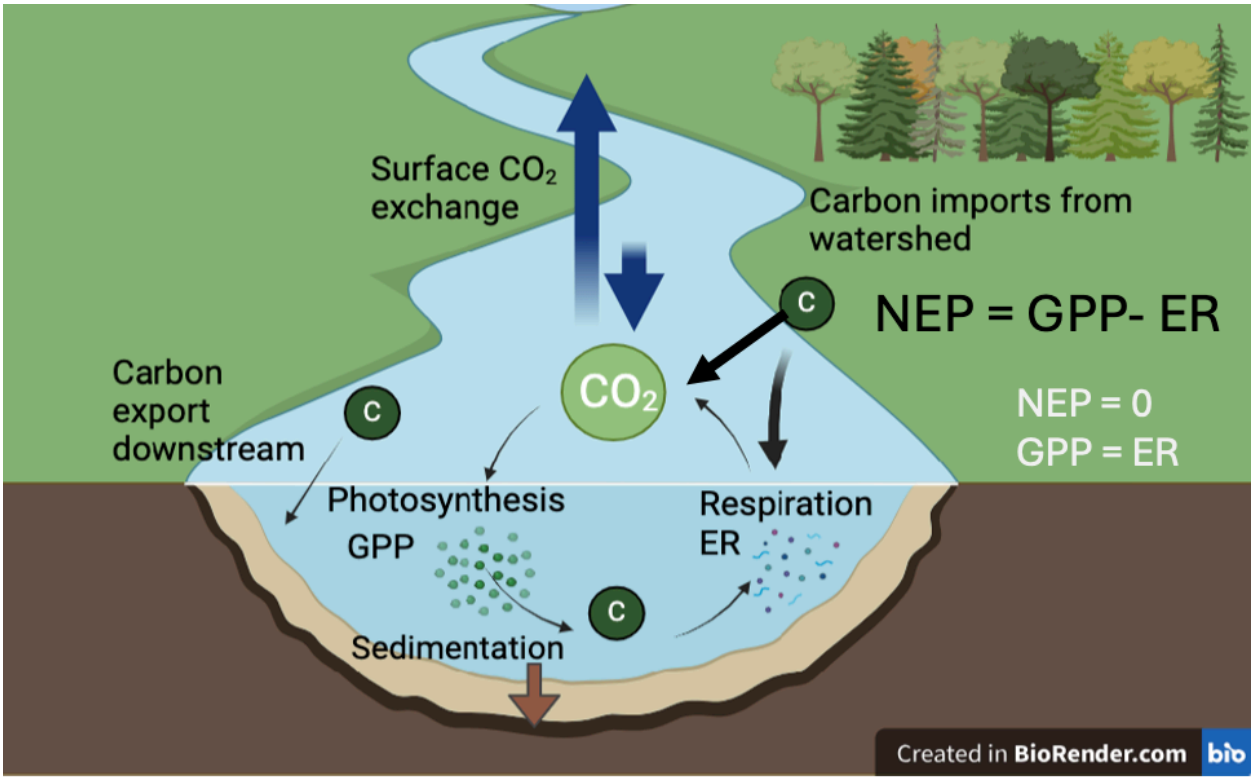

Figure 2. River C cycling and associated metabolic processes.

Climate changes that alter precipitation and runoff can affect the rate of OC loading into aquatic ecosystems. Many studies have shown trends of increasing coloured terrestrial dissolved organic matter (DOM), or DOC, content in aquatic ecosystems (Fig. 2), which is causing the browning of waters and is a growing concern for ecosystem functioning (Xenopoulos et al., 2021; McGovern et al., 2019). The browning of surface waters may enhance microbial processes and cause greater CO_2 emissions to the atmosphere (Fig. 2), modifying the rates of metabolism within these ecosystems (Lapierre et al., 2013). With wetter climates, it is predicted that OC concentrations in some regions will increase by 30-50% via increased flow over C-rich soils (de Wit et al., 2016). Terrestrial DOM content in aquatic systems is higher in wetter climate regions (Kellerman et al., 2014), and several studies have found that increased terrestrial aromatic DOM content is linked to greater CO_2 emissions (e.g., D'Amario and Xenopoulos, 2015). In other regions, including western Canada, multi-decadal observations show no evidence of directional changes in DOC flux in recent decades (Johnston et al., 2022). This suggests that riverine C cycling in semi-arid regions may function differently from better-studied rivers in temperate and boreal regions, with unclear effects of ongoing climatic change.

1.1.4. Research objectives

Given there is very little research on C cycling and river metabolism in western Canada, specifically southern Alberta, my project quantifies patterns of CO_2 emissions, C compositional shifts, and rates of metabolism in human-impacted rivers in southern Alberta, within the broader South Saskatchewan River watershed. One study has shown high rates of GPP in the mainstem of the Oldman River (Brinkmann and Rasmussen, 2012), yet no data exists for other metabolic rates, including ER or NEP, making it difficult to assess the metabolic balance and net C cycling in regional rivers. Based on the intense land use in this region, I hypothesize that an enhanced supply

of anthropogenic OM fuel negative rates of NEP and elevated CO_2 emissions. To test this hypothesis, my study has the following three objectives:

1) Track the spatial patterns of dissolved C composition, biodegradable DOC, and rates of CO_2 emissions.
2) Use high-frequency measurements of DO and discharge to model daily metabolic rates at select locations.
3) Use high-frequency pH sensor measurements with hydrological and routine sampling data to model rates of CO_2 emissions as well as their coupling to patterns of river metabolism.

CHAPTER 2. EXPLORING HUMAN IMPACTS ON RIVER METABOLISM AND CARBON CYCLING: A CASE STUDY IN THE LITTLE BOW RIVER, ALBERTA, CANADA

2.1 Introduction

2.1.1 Measuring metabolism to understand river ecosystem functioning

River metabolism encompasses the complex processes of OM production and consumption within lotic aquatic ecosystems (Fig. 2). The metabolism of a river is a vital indicator of ecosystem health and functioning. Measuring rates of metabolism can be utilized as a tool to evaluate ecosystem functions, including the transfer of energy (OM) and nutrients through photosynthesis and decomposition (Ferreira et al., 2020), and to identify disturbances or imbalances within an ecosystem linked to direct or indirect human impacts. The two fundamental metabolic rates of aquatic ecosystem metabolism are gross primary production (GPP), which involves autotrophic production (photosynthesis and chemoautotrophy) by plants and microbes, and ecosystem respiration (ER), which includes the mineralization of OM by autotrophs and heterotrophs (Bernhardt et al., 2018) (Fig. 2). The balance between rates of GPP and ER is termed net ecosystem production (NEP). Autotrophy and heterotrophy are terms that specify the net uptake or production of CO_2. The main internal ecosystem features that control river metabolism include light, temperature, flow, and nutrient concentration (Uehlinger, 2006; Bernot et al., 2010). These basic ecosystem physico-chemical properties are shaped by other factors such as hydrology and flow regime, riparian vegetation extent, and anthropogenic impacts (Bernhardt et al., 2022; Regnier et al., 2013). Therefore, various factors can impact river metabolism and food web CO_2 cycling, and these controls can change depending on the scale of the investigation.

2.1.2. Human impacts on metabolism and C cycling

Human activities that modify nutrient cycling have interactive effects on ecosystem C cycling. Land use can enhance the leaching of nutrients into aquatic ecosystems, which in turn may impact river metabolism (Bernot et al., 2010). Excess nitrogen (N) and phosphorus (P) loading can increase rates of GPP, enhance algal biomass, and shift C cycling by altering the rates of NEP (Fig. 2) (Bernot et al., 2010; Griffiths et al., 2013; Dodds & Smith, 2015). In a survey of river metabolism throughout the conterminous United States, rates of GPP varied more than rates of ER between regions (Bernot et al., 2010). Yet studies have shown diverse impacts of nutrients on river metabolism. One study in the Arctic tundra showed that increased nutrient concentrations shifted river metabolism to autotrophy (Peterson et al., 1985), while another study in a heavily shaded watershed in the Appalachian Mountains showed nutrients predominantly enhanced ER, which was attributed to terrestrial inputs (Rosemond et al., 2015). Where increased N and P content decreases NEP and enhances ER, this can contribute more CO_2 to the ecosystem and enhance emissions to the atmosphere (Cross et al., 2022). Ecosystem temperature can also impact the balance between autotrophy and heterotrophy, as NEP may decline with the warming of inland waters (Cross et al., 2022; Song et al., 2018). Removal of riparian vegetation can have multiple effects on GPP through reduced nutrient interception in runoff and increased light exposure. Shifts in the annual peak of ER or GPP due to alterations from land use or riparian shading may impact the ability of nutrients to be processed internally within river systems, thereby enhancing nutrient pollution (Bernhardt et al., 2018). Increased light exposure can enhance photosynthesis, and thus increase rates of GPP (Bernhardt et al., 2022). In urbanized areas with extreme nutrient pollution, a large portion of ER may be supported by sewage inputs rich in organic nutrients (Arroita et al., 2019). In a long-term study, ER decline of 50% was attributed to improvements in wastewater

treatment and greater OM removal (Uehlinger, 2006). Improving wastewater treatment can drastically lower CO_2 emissions from rivers, so it is imperative that the impact of upgrades to wastewater treatment are understood and implemented (Jarvie et al. 2020). Overall, human impacts on ecosystem properties can have diverse consequences for river metabolism.

Human modification of river hydrology impacts metabolism and C cycling in many ways. Damming changes the flow regime of the river by lengthening the water residence time in the catchment, in turn enhancing C processing on site (Maavara et al., 2021; Maavara et al. 2017). Modifications of river flow through damming can impact the thermal characteristics of the river network depending on the size and depth of the reservoir (Maavara et al., 2021; Tranvik et al., 2009). Temperature shifts can directly impact rates of river metabolism (Cross et al., 2022; Song et al., 2018). Introducing large flows can flood riparian sediments, which can increase nutrient and OM resuspension into rivers, and alter the cycling of C (Talbot et al., 2018; Brinkmann & Rasmussen, 2010). Damming also causes a shift in nutrient ratios that can impact phytoplankton communities in part by causing a shift to cyanobacterial dominance (Maavara et al., 2020). A transition to a more autotrophic, algal dominated river network can result in reduced CO_2 emissions in summer months due to enhanced GPP and C sequestration, potentially altering C emissions patterns from the network (e.g., Chan et al., 2023; Lapierre & del Giorgio, 2012). The impacts of reservoirs on river pCO_2 can vary, with some downstream river habitats showing lower, while others have elevated pCO_2 values (Yan et al., 2022). This exemplifies the need for more studies on a wide range of ecosystems and regions. Modifications to the flow rate of rivers also impact how fast nutrients may be processed or transported downstream (Ulseth & Hall, 2015; Deemer et al., 2022), with implications for downstream productivity. Short-term management of reservoir outflows can also impact food web functioning and possibly metabolism. Changes in

water level and hydropeaking impact fish and other aquatic organisms. Hydropeaking is the discontinuous release of water from reservoirs to match human electricity demands, which causes peaks in discharge (Greimel et al., 2018). Increased sediment mobilization linked to hydropeaking can impact aquatic organisms and displace them to lower-quality, downstream habitats (Greimel et al., 2018). Increased turbidity linked to hydropeaking can also decrease light availability and cause a decrease in rates of GPP (Hall et al., 2015; Deemer et al., 2022). Overall, there are various ways in which human modifications of river hydrology can alter river metabolism. These effects can have an impact on not only regional C cycling, but global C cycling as well, though these effects are complex, and not well understood.

2.1.3. Exploring metabolism and C cycling in understudied Canadian rivers

Most of our knowledge of human impacts and river functioning comes from select global regions. In general, river metabolism and C cycling in western Canadian rivers are understudied (Zhou et al., 2024). Human pressures, such as agriculture and urbanization, exert significant influences on water resources in the Canadian prairies (Schindler, 2001). Both agricultural and urban stormwater runoff can negatively impact river ecosystems due to excess nutrients, salts, and other pesticides that affect water quality (Little et al., 2003). In addition to this, water withdrawals due to irrigation and municipal needs impact river hydrology and flow, with implications for the internal processing of materials and food web functioning (Rood et al., 2005; Schindler and Donahue, 2006). With growing water demand in western Canada, the future of water security in the prairies is uncertain (Schindler & Donahue, 2006). It is necessary to explore the relationship between C cycling and water resources in southern Alberta, as human activities are impacting flow regimes in this region (Schindler, 2001). Understanding the influence of land use and flow regulation practices on

riverine metabolism can provide insights into food web functioning and riverine biogeochemistry. Here, I explore the patterns of metabolism and C cycling in a river network in southern Alberta that is heavily regulated and influenced by human stressors, which will ultimately provide new information on the functioning of western Canadian river ecosystems.

2.2 Methods

2.2.1. Study site

The Little Bow River (LBR) and Mosquito Creek (MC) are part of the Oldman River basin (ORB; Fig. 3), which has an overall area of 28,200 km^2 (Rock & Mayer, 2007). As one of the most heavily impacted watersheds in the region, the LBR drains 1963 km^2 of the mixed grassland subregion with a range of land use (Fig. 3) (Hillman et al., 2016). Land use in the LBR and MC watersheds includes urban and rural agricultural activities, with range land, native prairie, cattle operations, dryland farming, and irrigated cropland (Little et al, 2003). The LBR begins in the town of High River, where water is diverted from the Highwood River. In southern Alberta, many farmers and people depend on the LBR and MC as a water source for drinking water, agriculture, as well as recreational use for surrounding communities. The LBR alone is used for irrigation on more than 11,000 acres (4,400 hectares) of land (Rood et al., 2005). MC begins approximately 12 km southwest of the town of High River, where water is diverted from the Highwood River (Rood et al., 2005). A portion of this water is diverted into Clear Lake, and the remainder flows into Twin Valley Reservoir (TVR). Both the LBR and MC drain into the TVR (Fig. 3), which was constructed in 2003 and is one of the newest reservoirs in the province (Hillman et al., 2016; Rood et al., 2005). The TVR has experienced eutrophication since its construction, and there is concern that upstream nutrient loading is a main cause for this water quality loss (HMP-PAC, personal communication). Frank Lake is a restored wetland that receives effluent from both the town of High River and a local beef processing plant (White, 1999; Zhu et al., 2019). The Town of Nanton also discharges treated wastewater into MC. As Frank Lake drains into the LBR during wet years (Zhou et al., 2023), and MC receives effluent year-round, wastewater release and legacy nutrients

in the watershed potentially impact metabolic processes and C cycling throughout the river network.

Here, I used a combination of routine water sampling (in 2021 and 2022) at seven locations (see Appendix A for photos of each site location) in both the LBR and MCR and deployed autonomous sensors (in 2022) at three locations (Fig. 3). Water was collected from flowing habitats, and sensors were deployed in wadable locations. Sampling locations were generally chosen to represent the widest range of conditions and human impacts present throughout the watershed, including above and below the confluence with eutrophic water sources (Frank Lake outflow), above and below a constructed reservoir (TVR), above and below a diversion canal (on MCR). Most sites had corresponding hydrologic gauging stations (detailed below). On LBR, I sampled at five locations, and deployed sensors at the intersection with Highway 533 (LB533) and near the town of Carmangay (LBCAR) (Fig. 3). Each site is above and below the TVR, respectively. Water is diverted from the Highwood River (Bow River basin) to the Little Bow River in the town of High River, and I sampled immediately downstream from this canal as my uppermost watershed location (LBCAN). I sampled four additional sites on the LBR, including one location above the confluence with Peel Creek, which is the Frank Lake drain (LBUP), below the confluence at LB533, immediately below the TVR (TVRD) and at LBCAR (Fig. 3). The two sample sites on MCR included MCR and MCRDIV, which were respectively located above and below a canal diverting a subset of flow to nearby Clear Lake. Collectively, the sites span urban, cropland, rangeland, and native prairie habitats throughout the watershed.

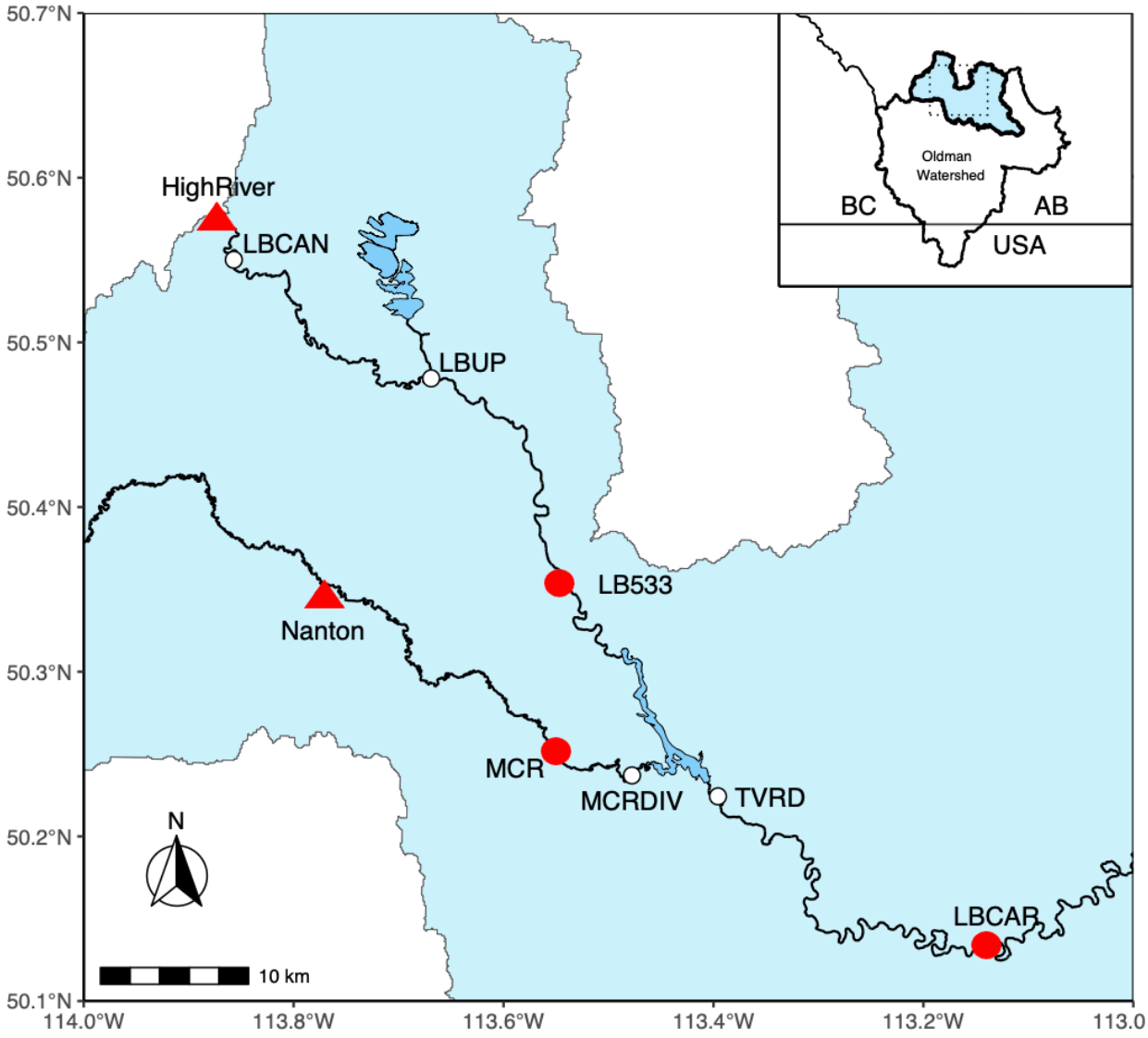

Figure 3. Location of the Little Bow River (LBR) and Mosquito Creek (MCR) in the Oldman Watershed, Alberta, Canada. Sampling sites are shown with white circles, and sites with sensor deployments are shown with red circles. The town of High River and Nanton are shown with red triangles. The Twin Valley Reservoir (TVR) is shown at the confluence of LBR and MCR. Inset, top right: Study site (black dashed box) in the Oldman Watershed, with the upper LBR Watershed in blue (see Appendix B for site latitude and longitude).

2.2.2. Water sample collection and field measurements

Routine water sampling took place biweekly to monthly from April to October in 2021 and 2022. Surface water samples were collected in 4-litre HCl-washed plastic containers and stored in ice-filled coolers during transportation to the lab for further processing. At the time of sampling, a YSI Exo1 sonde (Yellow Springs Instruments) was used to determine dissolved oxygen (DO) concentrations, DO percent saturation, pH, turbidity, water temperature, specific conductivity, salinity, and barometric pressure. The sonde was factory inspected before each Spring season and calibrated regularly for pH, turbidity, and specific conductivity and salinity. The sensor measuring DO concentration and DO percent saturation was calibrated daily on-site using local barometric pressure.

To obtain high-frequency (1 min resolution) water temperature and oxygen concentration data, MiniDOT (PME) sensors were deployed from May to October at LB533 and MCR, and from June to October at LBCAR. To estimate pCO_2 and model emissions rates, pH sensors (HOBO, model MX2501) were deployed at MCR and LB533 (Fig. 3). Sensors were attached to rebar that was pounded into the streambed at locations within ~50m of the nearby hydrometric gauging station, ensuring sensors were fully submerged throughout the measurement period. Sensors were factory-calibrated before deployment, and MiniDOT sensors were tested prior to deployment using an aerated ice bucket submersion method (not shown). All sensors were cleaned, and data was downloaded regularly during routine sampling.

2.2.3 Laboratory analyses

In the laboratory, unfiltered and filtered water samples were collected for further analysis. Water was filtered through high-capacity, 0.45µm capsule filters (Whatman) using a peristaltic pump. For measurement of dissolved organic and inorganic C concentrations (DOC, DIC, respectively), filtered water was stored in the dark at 4°C in pre-baked, 40 ml amber vials that were capped air-free with gas-tight liners. These samples were analyzed using a Shimadzu TOC-L high-temperature catalytic oxidation analyzer following standard lab protocols (Bogard et al., 2023).

As a proxy for the total amount of suspended phytoplankton biomass, chlorophyll *a* (Chl *a*) pigment concentrations were measured spectrophotometrically. Water samples were filtered through GF/F filters (nominal pore size 0.7µm, Whatman) and the particulate material on filters was frozen and stored in the dark until later analysis. Filters were then thawed and cut into strips, put into a glass vial, 5 ml of 90% acetone was added, and samples were held in storage in the dark at -20°C for 24 hours. The extract was then filtered using lock-on syringe filters (0.22 um) and transferred to baked glass vials. To determine the total amount of pigment, absorbance was measured using a Biochrom Ultrospec 3100 pro spectrophotometer. The samples were completed at room temperature using a 1 cm quartz cuvette. Wavelengths measured included 480, 630, 645, 665, and 750 nm and calculations of Chl *a* followed Jeffrey and Humphrey (1975).

$$Chl\ A\ \mu g\ L^{-1} = \left(11.85(A_{665} - A_{750}) - 1.54(A_{645} - A_{750}) - 0.08(A_{630} - A_{750})\right) \times \frac{E}{V} \quad (1)$$

Where E is the volume of the extraction solvent (mL) and V is the total volume filtered (L).

2.2.4. Bioavailable DOC (BDOC) incubations

In August 2022, I used standard incubations to determine the content of bioavailable DOC (BDOC) available to the microbial community. I conducted a standardized 28-day incubation for water samples collected from all sites. The incubations were set up in a triplicate (a total of 21 incubations) following Vonk et al. (2015) but modified following Zhou et al. (2023) by filtering water using a 0.2µm pore sized filter (PALL Supor 200) instead of 0.7 µm. To start the incubation, filtered water was added into pre-combusted 1L amber bottles. Next, I added a 1% (by volume) microbial inoculation to filtered water, which consisted of water that was filtered using GF/D filters (1.2 µm nominal pore size; Whatman). I stored all incubations in the dark at room temperature for the duration of the experiment. I collected microbe-free filtered samples on days 0, 2, 7, 14, 21 and 28 for measurement of DOC concentrations, to explore the loss of DOC through time (detailed above, following Bogard et al. 2023). A total of 126 samples were processed. BDOC loss in mg L^{-1} was defined as the difference in concentration of DOC from day 0 to day 28, and BDOC percent loss (%) as the percentage of DOC concentration remaining on day 28 relative to the initial DOC concentration. Values exceeding 100% represent cases where DOC content increased during incubations.

2.2.5. Hydrological data

The discharge values, mean river channel depth, width, and velocity data were obtained from both federal and provincial monitoring sources, from both the federal database (https://wateroffice.ec.gc.ca/mainmenu/real_time_data_index_e.html) and the Alberta River Basin website for provincially-monitored sites (https://rivers.alberta.ca/). The gauging stations IDs were:

05BL015- Little Bow Canal at High River (LBCAN), 05AC930- Little Bow River at Highway No. 533 (LB533), 05AC031-Mosquito Creek near the Mouth (MCR), 05AC937-Mosquito creek below Clear Lake Diversion (MCRDIV), 05AC941-Little Bow River below Twin Valley Reservoir (TVRD), and 05AC003-Little Bow River at Carmangay (LBCAR). To estimate the mean depth, cross-sectional depth measurements were obtained from government sources for every month of 2022, and averaged to obtain mean cross-sectional river depth at each gauged location (Appendix Fig. C1). Mean depth was then regressed against daily discharge to obtain a relationship that enabled us to estimate mean channel depth measurements based on higher frequency discharge measurements. Velocity data were also obtained, and a similar velocity-discharge regression model was created for each site to obtain high frequency velocity measurements (Appendix Fig. C2). For the LBUP site, there was no gauging station directly there, so we used the discharge and velocity from the closest upstream site, LBCAN. In addition, the LBCAN site did not have a gauging station directly where sampling occurred but was roughly 5 km downstream from the gauging station that was used for calculations and modeling.

2.2.6. Estimating CO_2 content and emissions

I calculated the concentration of CO_2 (in mmol L^{-1}) in the water following Aberg & Wallin, (2014). For routine, lower frequency sampling, I used the concentrations of DIC (methods detailed above), combined with sonde measurements of pH and water temperature to calculate the fraction of DIC present as CO_2 using equation 1:

$$CO_2 = \left(\frac{DIC}{1 + \frac{K_1}{H} + \frac{K_1 K_2}{H^2}} \right) 10^6 \quad (2)$$

$$K_1 = 10^{\left(\frac{-3404.71}{T}+14.8435-0.032758T\right)} \quad (3)$$

$$K_2 = 10^{\left(\frac{-2902.39}{T}+6.498-0.2379T\right)} \quad (4)$$

$$pCO_2 = \frac{CO_2}{S_{CO2}} \quad (5)$$

$$S_{CO2}=10^{\left(-\left(\frac{-9345.17}{T}-60.2409+23.3585\log\frac{T}{100}+Sal\left(0.023517-0.023656\left(\frac{T}{100}\right)+0.0047036\left(\frac{T}{100}\right)^2\right)/\log 10\right)\right)} \quad (6)$$

Where H is the hydrogen ion concentration, and K_1 and K_2 are equilibrium constants in equations 1 and 2. To determine the CO_2 in the water, I used equation 1 together with pH and the equilibrium constants (equations 2 and 3). Next, with equation 4, I used CO_2 concentrations from equation 1 and S_{CO2} from equation 5 to calculate pCO_2 (µatm). I determined the solubility of CO_2 (S_{CO2}) using equation 5 following Weiss (1974), where T is water temperature in Kelvin. For high frequency measurements using pH sensors, I interpolated daily DIC concentrations from the biweekly to monthly grab samples.

To calculate the rates of CO_2 emissions on each date (F_{CO2}), I used equation 6 in combination with equations 7 to 10:

$$F_{CO2} = k_{CO2}Kh(pCO_2 - pCO2_a) \quad (7)$$

$$Kh = 10^{-(1.11+0.016T-0.00007T^2)} \quad (8)$$

$$k_{CO2} = \left(\frac{Sc}{600}\right)^{-\frac{1}{2}} k_{600} \quad (9)$$

$$Sc = 1911 - 118.11T + 3.453T^2 - 0.0413T^3 \quad (10)$$

$$k_{600} = 4725(VS)^{0.86} Q^{-0.14} D^{0.66} \quad (11)$$

Here, F_{CO2} is the rate of emissions (g C m^{-2} d^{-1}), pCO_2 and pCO_{2a} are the partial pressures of CO_2 observed and at equilibrium with the atmosphere, respectively, k_{CO2} is the gas transfer coefficient for CO_2 (m d^{-1}), *K*h is Henry's constant calculated following Wang et al. (2021) using equation 7, where *T* is water temperature in degrees Celsius. I calculated k_{CO2} using equation 8, where *Sc* is the Schmidt number, specific for CO_2 (equation 10), k_{600} is the gas transfer velocity standardized to an *Sc* of 600, and the negative ½ exponent is used following Raymond et al. (2012). I calculated *Sc* using equation 10, following Wanninkhof (1992). I calculated k_{600} using equation 11, which was taken from Raymond et al. (2012) (their equation 7). *V* is velocity (m s^{-1}), *S* is slope (unitless), *Q* is discharge (m^3 s^{-1}), and *D* is mean cross-sectional depth (m). For *V*, *Q* and *D*, I derived them as detailed above. Slope was derived in Google Earth, by calculating the change in elevation over the stream reach, using a standardized length for each site (1 km).

2.2.7. Modelling river metabolism

I estimated rates of GPP, ER, and NEP from diel DO and temperature data from miniDOT sensors. Following equation 12, I used the inverse modelling approach within the *streamMetabolizer* package in R (Appling et al, 2018a), that uses Bayesian parameter estimation as well as a

hierarchical state space modelling framework to generate daily estimates of GPP, ER, and k_{600d} (derived from *streamMetabolizer*) (Appling et al, 2018b). These estimates are generated by the best fit between modeled and observed DO data. Model convergence was visualized using *traceplot* in the rstan package (Stan Development Team, 2022), to determine the correct number of burn in steps (500) with 3000 Markov chain Monte Carlo steps from four chains after burn-in to decrease equifinality between GPP, ER, and k_{600d}. I constrained the variability in k_{600d} by binning the range of possible estimates linked to discharge (O'Donnell and Hotchkiss, 2019). I removed all metabolism estimates that were not biologically possible, including negative GPP or positive ER values. I next removed days of data that had poor chain convergence or model fit, specifically when days had Rhat values that exceeded 1.1 and when N_eff values exceeded 12,000, which is the total number of saved steps (3000) multiplied by the number of chains (4) (O'Donnell and Hotchkiss, 2019). A total of 6 days were removed, resulting in 90 days of quality checked GPP and ER data for each site, or a total of 270 days combined between the three sites. The base equation for *streamMetabolizer* is as follows (equation 12; Appling et al,2018a):

$$\frac{dO_{i,d}}{dt} = \left(\frac{GPP_d}{\bar{z}_{i,d}} \times \frac{PPFD_{i,d}}{PPFD_d}\right) + \left(\frac{ER_d}{\bar{z}_{i,d}}\right) + f_{i,d}\left(k_{600_d}\right)\left(Osat_{i,d} - O_{i,d}\right) \quad (12)$$

Where $O_{i,d}$ is the modeled oxygen concentration on day d and time index i, and $dO_{i,d}/dt$ is the rate of concentration change. GPP_d, ER_d, and k_{600d} are the daily parameters that are fitted by the model. GPP_d and ER_d (g O_2 m^{-2} d^{-1}) are the daily metabolic rates, and k_{600d} is the daily standardized gas exchange rate coefficient (d^{-1}, scaled to a Schmidt number of 600). The other variables are the inputs for the model: $\bar{z}_{i,d}$ is the stream depth(m), $PPFD_{i,d}$ is the photosynthetic photon flux density (μmol photons m^{-2} d^{-1}), and the $PPFD_d$ is the daily mean of $PPFD_{i,d}$. $f_{i,d}\left(k_{600_d}\right)$ is a function

that converts the mean k_{600d} to an oxygen specific, temperature-specific, gas exchange coefficient, and the $Osat_{i,d}$ is the theoretical saturation of O_2 if the water and air were in equilibrium.

2.2.8. Numerical analyses

All statistical analyses were computed in R version 4.2.0 (v4.2.0; R Core Team 2022). I assessed the normality of data distributions visually using histograms in conjunction with Quantile-Quantile plots (*qqplot*). I used a one-way analysis of variance (ANOVA) with Tukey's honestly significant difference post hoc tests (*Tukey_HSD*) to compare values of DOC, pCO_2, F_{CO2}, and k_{600} between routine sampling locations. Prior to analysis, I $\log_{10}$-transformed pCO_2 and F_{CO2} to meet assumptions of normality of distribution, and square root transformed values of k_{600}. I used a Kruskal-Wallis test (*kruskal.test*) with a Dunn post-hoc test (*dunn.test*) for DIC, BDOC values, and %BDOC as they were not normally distributed and could not be successfully transformed as for other parameters. For mean depth and velocity calculations, all regression amylases were conducted using Ordinary Least Squares Regression on untransformed or $\log_{10}$-transformed data. Where boxplots are shown, the boxes represent the first to third quartile, or the interquartile range (IQR), with the midline as the median value, and the vertical lines extend from the largest to smallest values that are within 1.5 times above or below the IQR. Individual points outside of this range are shown as outliers.

2.3. Results

2.3.1. Hydrologic and limnological conditions across sample sites

The hydrologic conditions at all sites were heavily regulated through canal diversions and irrigation withdrawal, and therefore had relatively low flow rates, and did not follow predictable seasonal trends (Fig. 4). The maximum discharge rate measured in the network in 2021 and 2022 was 7.9 $m^3 s^{-1}$ at LBCAN (Fig. 4a, Table 1) and the minimum was 0.2 $m^3 s^{-1}$ at MCRDIV (Fig. 4d, Table. 1). The mean discharge rate for all sites was 2.73 $m^3 s^{-1}$. The seasonality of discharge was extremely variable and unpredictable (Fig. 4), with frequent water withdrawals throughout the year. The minimum mean channel depth was 0.09 m at MCRDIV (Fig. 4j) and the maximum mean depth was 1.16 at LBCAN (Fig. 4g). The mean depth for all sites was 0.45 m. Between 2021 and 2022, similar patterns were generally observed. Brief periods did occur where flow differed between years at LBCAN, LB533, and TVRD (Fig. 4a, b, e, respectively).

Concentrations of DO were consistent across sites (averaging from 9.6 mg L^{-1} at LBCAN, to 11.2 mg L^{-1} downstream at LBCAR; Table 1). Yet DO concentrations ranged widely within sites through time (the smallest and largest ranges within sites were 7.7 and 16.4 mg L^{-1}, respectively). In contrast, I found that water temperature varied considerably within and across sites. The highest mean temperature of 18.9 ºC was found at MCRDIV, and the lowest mean temperature of 13.2 ºC was found at LB533 (Table 1). Concentrations of Chl *a* were generally low (mean = 1.5 $\pm$ 1.8 µg L^{-1} and range of 0 to 10.6 µg L^{-1}; Table 1). The highest Chl *a* concentration was 10.6 µg L^{-1} and was observed at LB533 during July of 2021.

Table 1. Physical and chemical conditions measured at each sampling location. Values summarise all data collected in 2021 and 2022. See text and figure 3 for abbreviation definitions. Values presented include mean ± 1 S.D. and range of values are presented in parentheses.

	LBCAN	LBUP	LB533	MCR	MCRDIV	TVRD	LBCAR
Temperature (ºC)	14.1 ± 3.8 (8.3-18.7)	13.5 ± 5.9 (0.5-20.9)	13.2 ± 6.5 (0.1-21.0)	14.7 ± 6.7 (0.0-22.2)	18.0 ± 4.9 (9.8-23.1)	14.4 ± 5.4 (2.9-21.9)	18.9 ± 4.3 (11.8-23.8)
DO ($mg\ L^{-1}$)	9.6 ± 0.7 (8.8-10.9)	9.8 ± 1.4 (7.9-12.9)	10.0 ± 1.7 (7.7-13.6)	10.5 ± 2.0 (7.7-16.4)	10.1 ± 1.4 (8.9-12.9)	10.9 ± 1.1 (9.6-13.4)	11.2 ± 1.7 (8.9-13.2)
pH	8.1 ± 0.2 (7.9-8.4)	8.2 ± 0.2 (7.8-8.5)	8.2 ± 0.2 (7.6-8.4)	8.4 ± 0.2 (8.0-8.7)	8.3 ± 0.2 (8.1-8.6)	8.4 ± 0.2 (7.9-8.8)	8.5 ± 0.3 (8.1-8.8)
DIC ($mg\ L^{-1}$)	31.3 ± 3.2 (26.7-34.5)	34.9 ± 5.1 (28.6-46.1)	34.2 ± 5.0 (26.2-44.8)	37.2 ± 13.6 (24.6-79.7)	29.9 ± 5.9 (23.7-36.4)	38.1 ± 10.3 (26.1-73.9)	29.6 ± 3.4 (26.2-35.3)
DOC ($mg\ L^{-1}$)	2.5 ± 1.7 (1.3-5.5)	3.0 ± 2.9 (1.0-15.1)	2.3 ± 0.7 (1.4-4.0)	3.6 ± 1.6 (1.7-7.9)	3.7 ± 1.5 (2.0-5.9)	3.8 ± 0.7 (2.9-5.1)	3.6 ± 0.5 (3.3-4.5)
Chl *a* ($\mu g\ L^{-1}$)	0.3 ± 0.2 (0.1-0.6)	1.2 ± 1.2 (0.1-4.0)	1.6 ± 2.2 (0.0-10.6)	1.5 ± 1.5 (0.3-6.5)	1.0 ± 0.7 (0.5-2.3)	2.3 ± 2.5 (0.2-9.6)	0.9 ± 0.4 (0.3-1.4)
pCO_2 (µatm)	938.0 ± 332.6 (573.7-1370.6)	1070.8 ± 562.8 (527.0-2739.7)	1174.3 ± 656.7 (549.9-3010.9)	720.8 ±282.8 (334.0-1159.8)	629.6 ±321.5 (298.1-1021.9)	822.6 ± 503.4 (275.1-2228.9)	520.0 ± 465.5 (212.9-1315.4)
Discharge ($m^3\ s^{-1}$)	3.5 ± 2.6 (0.6-7.8)	3.5 ± 2.3 (0.6-7.9)	2.9 ± 1.3 (0.8-5.4)	1.3 ± 0.4 (0.2-1.9)	0.7 ± 0.5 (0.2-1.3)	3.3 ± 2.1 (0.3-7.1)	2.5 ± 0.7 (1.4-3.2)
k_{600} ($m\ d^{-1}$)	7.9 ± 2.5 (5.4-12.0)	7.4 ± 2.1 (5.1-11.5)	4.5 ± 1.1 (2.9-6.7)	3.0 ± 0.8 (0.9-4.3)	2.2 ± 0.9 (1.2-3.4)	5.8 ± 3.0 (1.7-11.4)	5.2 ± 0.9 (3.9-6.2)
F_{CO2} ($mmol\ m^2\ d^{-1}$)	68.6 ± 38.2 (12.9-96.9)	98.2 ± 116.3 (9.0-506.2)	65.2 ± 68.5 (11.2-269.7)	16.1 ± 18.4 (-6.8-51.6)	9.7 ± 13.0 (-3.6-21.4)	31.6 ± 44.7 (-32.7-143.4)	13.0 ± 48.0 (-23.4-94.6)

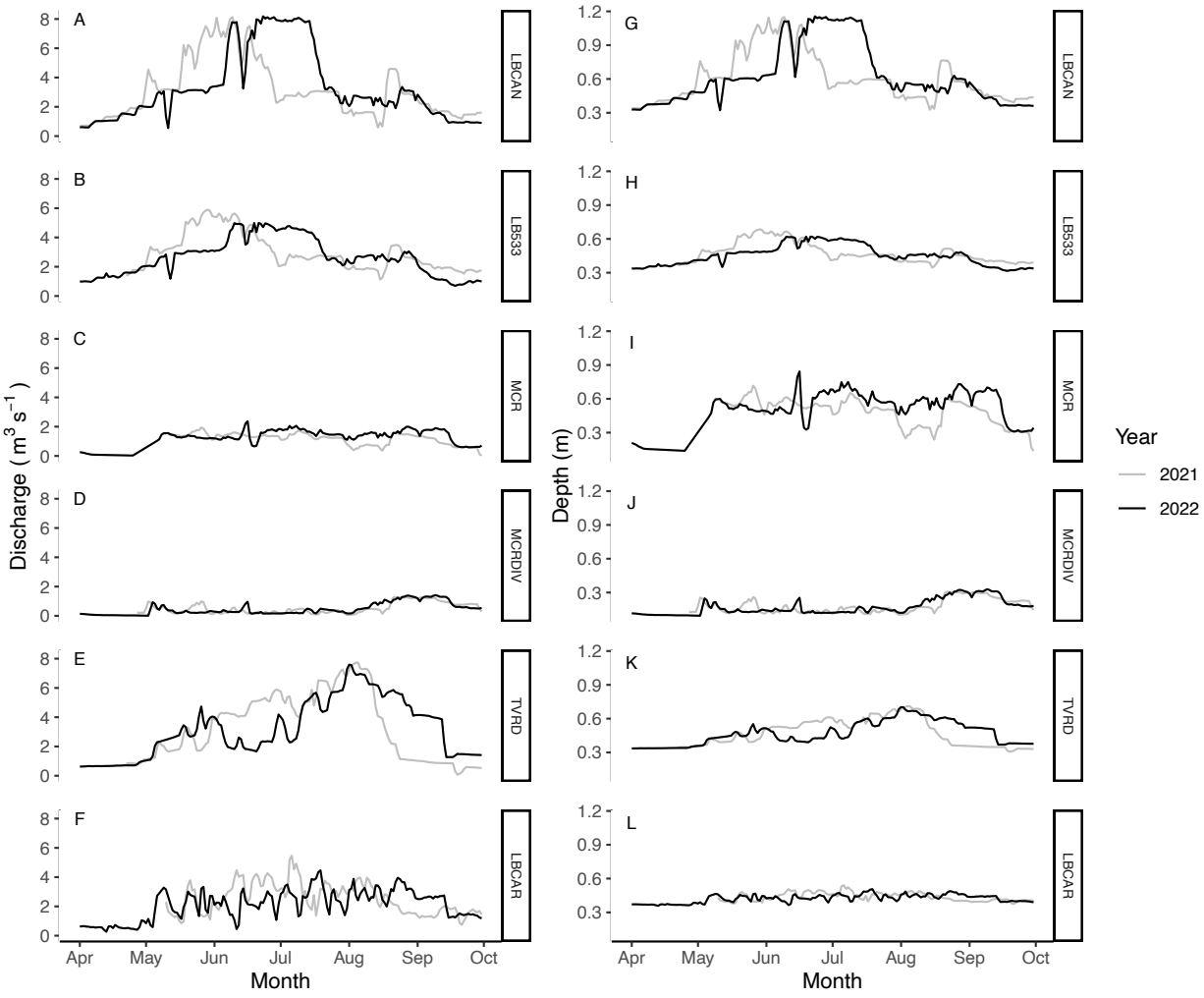

Figure 4. Daily average discharge rate and mean cross-sectional depth of water in the river channel at each sampling location. See Figure 3 for site locations and text for the definition of abbreviations.

I found little difference in most chemical and physical conditions among sites. From up to downstream, all sites had elevated DIC concentrations ranging from 23.7 to 79.7 mg L^{-1} (mean ±1 S.D. = 35.1 $\pm$ 8.8; Table 1, Fig. 5a). There was no significant difference between sites for concentrations of DIC (Kruskal-Wallis, χ^2 = 11.3, p = 0.08). Across sites, concentrations of DOC averaged 3.2 $\pm$ 1.8, ranging from 1.0 to 15.1 mg L^{-1} (Fig. 5b, Table 1). I observed significant differences in DOC concentrations between sites (ANOVA: p = 7.5e-05, F = 5.4), with sites on MCR and below the TVR generally elevated in DOC concentrations (Fig. 5b). On one occasion, I found elevated DOC concentrations of 15.13 mg L^{-1} at LBUP (June 2022). For ratios of DIC:DOC (Fig. 5c), there were significant differences among sites (ANOVA, F = 5.028, p = 0.00016). The DIC:DOC ratios decreased from upstream to downstream, as LBCAR had the lowest ratio (mean = 8.2 $\pm$ 0.6 and LBCAN had the highest ratio (mean = 16.7 $\pm$ 8.0). All sites were alkaline, with pH values ranging from 7.6 to 8.8 (mean = 8.3 $\pm$ 0.24, Table 1, Fig. 5d). From up – to downstream, values of pH trended upwards (ANOVA, F = 6.35, p = 8.32e-06).

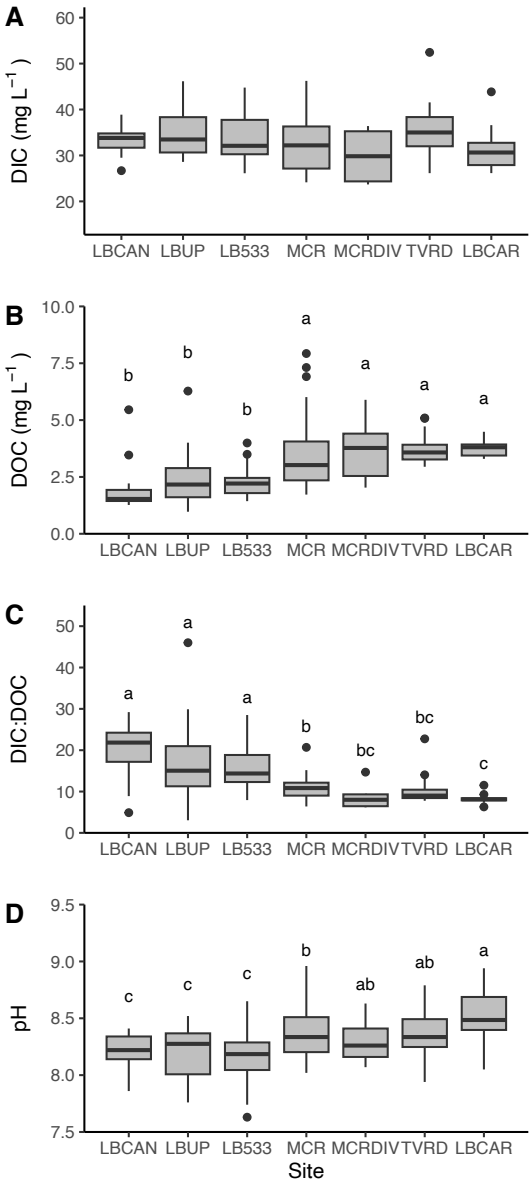

Figure 5. Carbon content and pH were measured at each sampling site in 2021 and 2022. DIC (a), DOC concentrations (b), the ratio of DIC:DOC (c), and pH (d) were compared among sites. Lowercase letters denote post-hoc groupings (Tukey HSD; significance at $p < 0.05$). Sites are ordered from most upstream on the left to downstream on the right. See Figure 3 for site locations and text for the definition of abbreviations.

2.3.2. BDOC incubation experiment

Microbial DOC consumption in standardized incubations decreased from upstream to downstream across sites (Kruskal-Wallis: $\chi^2 = 12.3$, $p = 0.0005$), with mean values of 1.36 mg L^{-1} for the overall BDOC loss over 28 days and ranging from -0.15 downstream at TVRD to 3.52 mg L^{-1} upstream at LBCAN (Fig. 6). At TVRD, the negative value indicates a small gain in BDOC. There was a significant difference between upstream sites and downstream sites for BDOC loss (Kruskal-Wallis: $\chi^2 = 12.27$, $p = 0.0005$). The maximum %BDOC loss was 71.3% at LBCAN, and the minimum was -4% at TVRD, for which incubations gained BDOC. The mean %BDOC loss for all the sites was 35.9% $\pm$5.7. Below the TVR, the %BDOC loss was drastically lowered at TVRD but increased again further downstream at LBCAR. Consequently, there was a significant difference between sites for %BDOC loss (Kruskal-Wallis: $\chi^2 = 16.2$, $p = 0.013$)

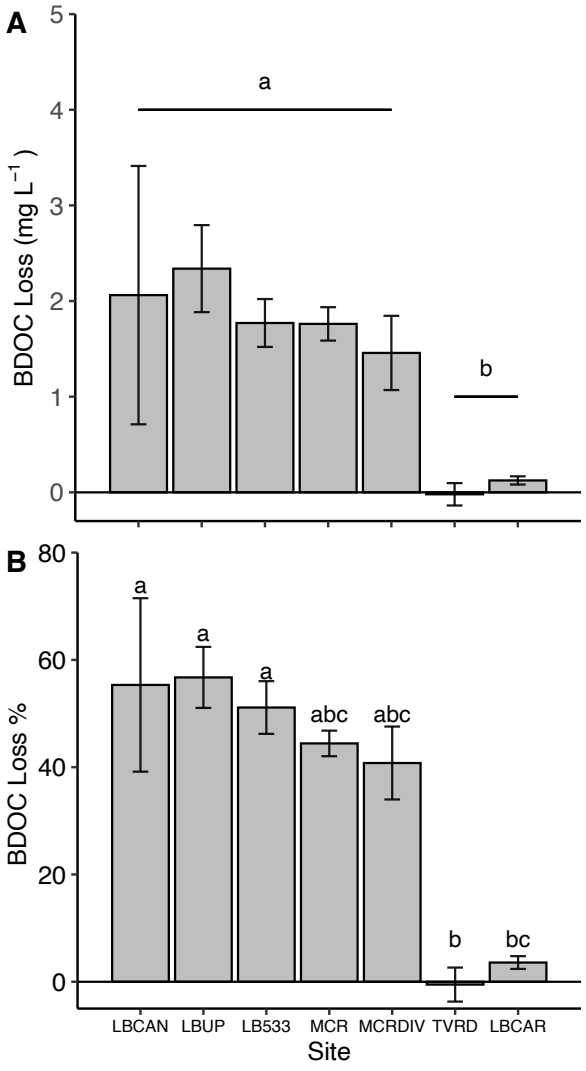

Figure 6. Microbial BDOC incubations were conducted in August 2022. BDOC loss over 28 days in mg L^{-1} (a) and %BDOC loss (b). Averages and error bars (1 S.D.) summarize triplicate incubations for each site. Lowercase letters denote post-hoc groupings (Dunn test; significance at $p < 0.05$).

2.3.3. Across site patterns of CO_2 content and flux

Values of pCO_2 at the sites were generally low, averaging 913.8 $\pm$ 532.8 µatm, and ranging from 212.9 at LBCAR to 3010.9 µatm at LB533 (Table 1, Fig. 7a). There was a decreasing trend in pCO_2 from upstream to downstream, with significant differences between sites (ANOVA: F = 4.18, p = 0.001). LBUP and LB533 had the most extreme values (i.e., more outliers) compared to other sites. The corresponding k_{600} values calculated on each sampling date following Raymond et al. (2012) had a mean of 5.3 $\pm$ 2.6 m d^{-1} (Table 1, Fig. 7b) and ranged significantly (ANOVA: F = 18.9, p = 6.54e-15), from 0.91 to 12 m d^{-1}, decreasing to lowest average values at LB533 and in MCR at both locations, and increasing to highest values of 12 at LBCAN. Below the TVR, k_{600} values increased at TVRD and decreased again at the downstream site LBCAR. The maximum rates of CO_2 emissions (F_{CO2}) based on low-frequency sampling were observed at LBUP (6.1 g C m^2 d^{-1}), and the minimum was -0.4 g C m^2 d^{-1}at TVRD (Table 1, Fig. 7c). There were modest but significant differences between sites for F_{CO2} (ANOVA: F = 2.78, p = 0.017), and rates of emissions generally decreased moving downstream. But in general, the only sites with significant differences were MCR and LBUP (Fig. 7c).

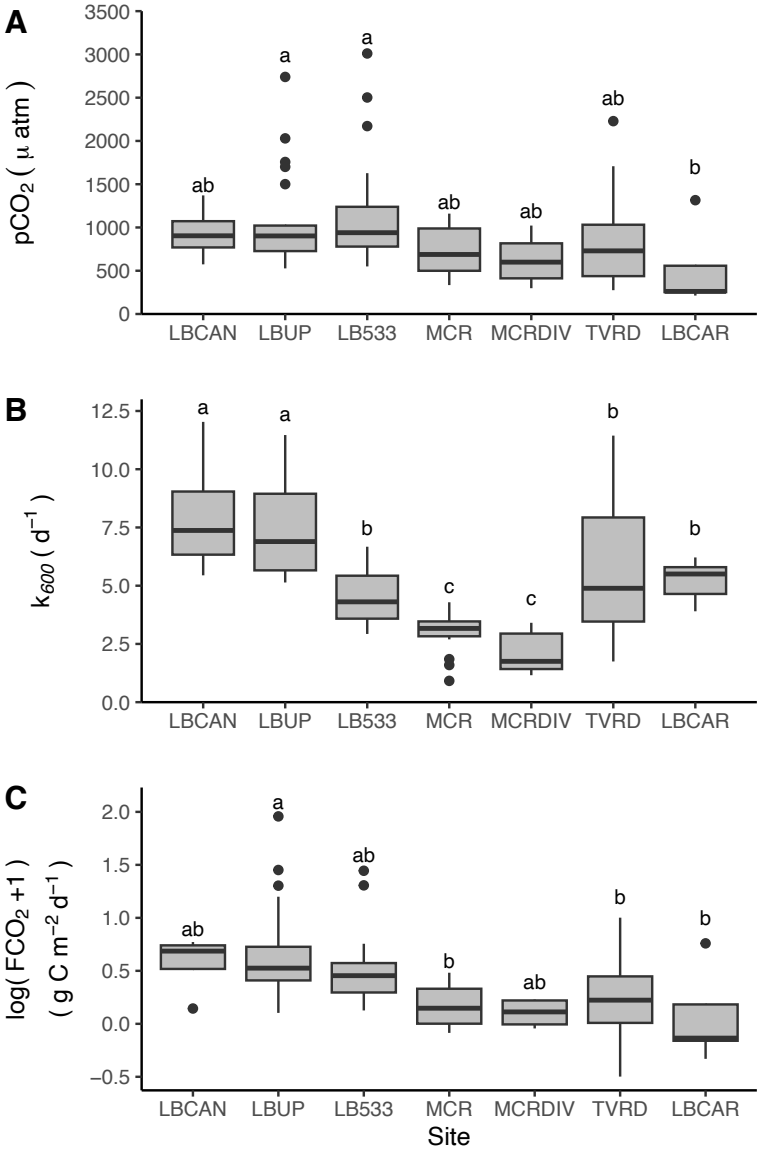

Figure 7. Spatial patterns of pCO_2 (panel a), k_{600} (panel b), and F_{CO2} (panel c). Note that F_{CO2} is presented as log-transformed values. Significant differences among groups from the ANOVA (post hoc: Tukey HSD) are shown as lowercase letters ($p < 0.01$).

2.3.4. High-frequency CO_2 content and fluxes

The high-frequency measurements of pH, CO_2 content, and emissions differed between sites and seasons (Fig. 8). The pH was alkaline at both sites; mean pH at LB533 was 8.36 + 0.22 (Fig. 8a), and at MCR mean pH was 8.54 + 0.33 (Fig. 8b). Values ranged from a maximum pH of 9.1 and minimum of 7.92, both at MCR. The pH at LB533 varied less throughout the year in comparison to MCR, where there was a decrease in pH in the middle of August, then began to increase from September to October. Values of pCO_2 were supersaturated relative to atmospheric values for most of the year at LB533 (Fig. 8c), with a mean pCO_2 of 705.5 $\pm$ 328.0, ranging from 204.8 to 1633 µatm (Fig. 8d). In comparison, MCR had lower mean pCO_2 of 520.5 + 382.6 µatm, ranging from 92.8 to 1780.4 µatm. The values of k_{600} calculated following Raymond et al. (2012) also differed between sites, but both followed a similar trend, decreasing from July to October (Fig. 8e, f). The mean k_{600} was 4.3 d^{-1} ranging from 2.9 to 6.3 d^{-1} and 4.4 $\pm$ 1.1 d^{-1} ranging from 1.9 to 7.1 d^{-1} for LB533 and MCR respectively. MCR had more drastic, short-term changes in k_{600}, likely due to changes in irrigation withdrawal that impacted water level and discharge. During mid-September, k_{600} dropped at MCR, as the discharge was nearing zero (Fig. 8f). LB533 had similar water drawdowns, though not as frequent throughout the year. The fluxes between both sites were similar, with the mean F_{CO2} of 0.1 $\pm$ 0.42 g C m^{-2} d^{-1} ranging from -0.25 to 1.0 g C m^{-2} d^{-1} and 0.3 $\pm$ 0.4 ranging from 0.017 to 0.76 g C m^{-2} d^{-1}.

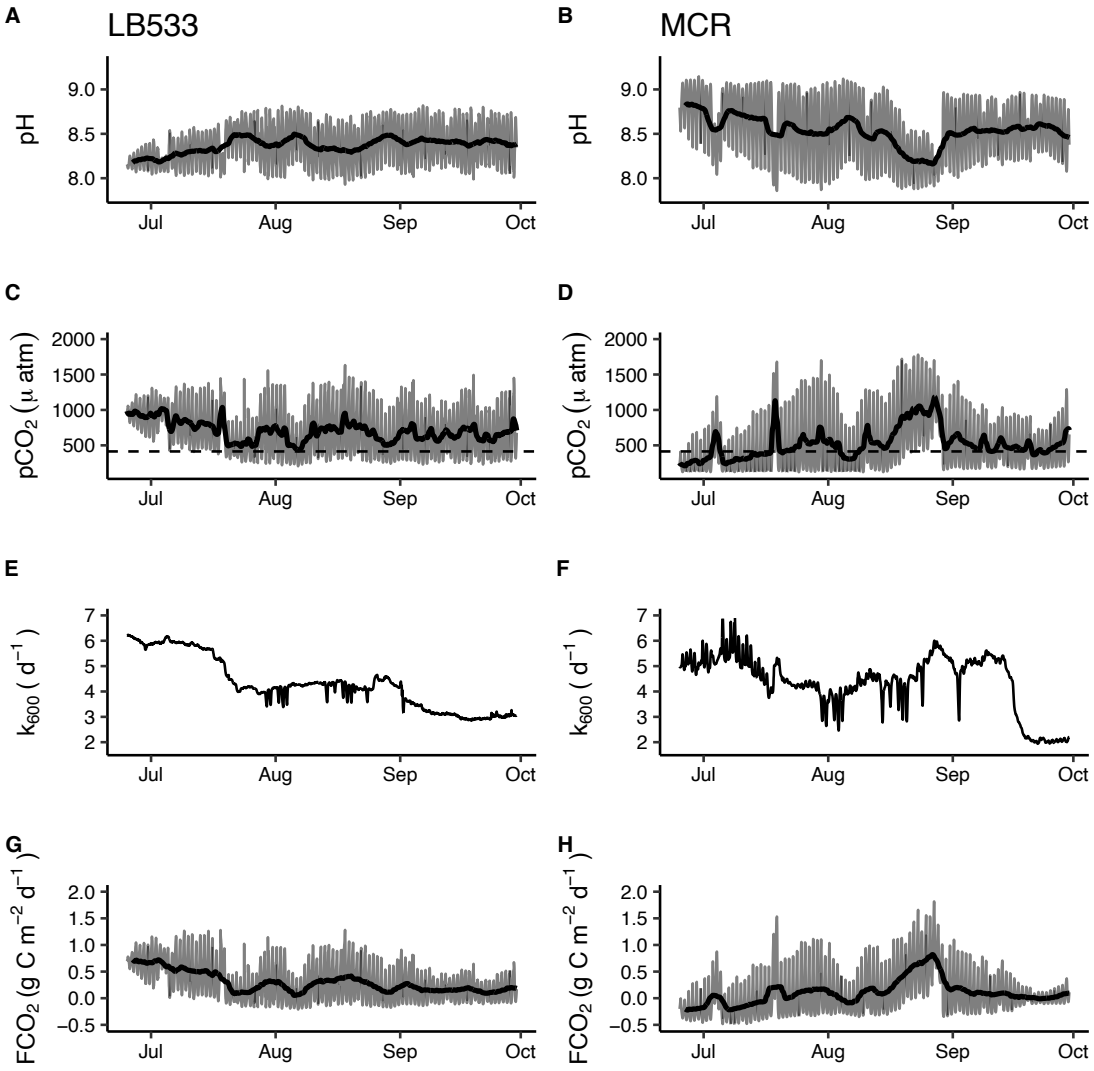

Figure 8. Calculated high frequency (grey) and moving average (black) for pH (panel a and b), pCO_2 (panel c and d),and F_{CO2} (panel g and h) for LB533 and MCR respectively, as well as calculated high frequency k_{600} (panel e and f).

2.3.5. Modelled estimates of GPP, ER, and NEP for each site.

The metabolic rates were similar between sites (Table 2), but the trends differed among sites (Fig. 9). Across all sites, the mean (±1 S.D.) GPP was 3.2 ±1.7, ranging from a low of 0.5 at LB533 to a high of 7.2 g O_2 m^{-2} d^{-1} at MCR (Table 2, Fig. 9). MCR had the highest rates for both GPP and ER, while LB533 had the lowest. The mean rates of GPP were 2.0 ± 0.9, 4.3 ± 1.5, and 3.4 ± 1.5 g O_2 m^{-2} d^{-1} for LB533, MCR, and LBCAR, respectively. Across sites, the mean rate of ER was -3.5 ± 1.5, while the greatest rate was calculated to be -7.9 g O_2 m^2 d^{-1} at MCR, and the lowest was 0 g O_2 m^2 d^{-1} at LB533. The mean NEP across all sites was -0.24 ± 0.62 and ranged from -2.8 g O_2 m^2 d^{-1} at LB533 to 2.0 g O_2 m^{-2} d^{-1} at MCR. The mean NEP was 0 g O_2 m^{-2} d^{-1} for both MCR and LBCAR, while LB533 was -0.7 g O_2 m^{-2} d^{-1}. This suggests that GPP and ER were in close balance at MCR and LBCAR, with neutral net metabolism, while LB533 had greater rates of ER than GPP and was overall heterotrophic.

Based on seasonal trends, LB533 had an increase in GPP at the beginning of July, but rates declined in mid-July and remained relatively stable at low values until September (Fig. 9a). For rates of GPP at MCR (Fig. 9b), there was a steady increase beginning in spring, reaching a plateau in July, where it then steadily decreased starting in August (Fig 9b). LBCAR had a different trend, starting with high GPP in June, and decreasing for the rest of the year (Fig 9c). Trends in the rates of ER generally mirrored those of GPP (Fig. 9a-c). The rates of GPP and ER were typically closely coupled each day for both MCR and LBCAR (Pearson correlation: r = -0.94, p = 2.2e-16, and r = -0.99, p = 2.2e-16, respectively) (Fig. 10). For LB533, rates of GPP and ER were less tightly coupled (r = -0.79, p = 2.2e-16).

The trends in NEP were similar for both MCR and LBCAR, with fluctuations near 0 g O_2 m^2 d^{-1} the whole year (Fig. 9b, c). In contrast, LB533 had negative rates of NEP from the beginning

of the year with an increase towards August, where then larger negative peaks of NEP occurred until the end of September (Fig. 9a). Overall, there were variable trends in GPP, ER, and NEP, yet MCR and LBCAR followed similar trends for NEP, differing from LBR.

Table 2. Metabolic rates (g O_2 m^{-2} d^{-1}; mean ± S.D.) for each sample site. Abbreviations defined in text.

	LB533	MCR	LBCAR
GPP	2.0 ± 0.9 (0.5-4.7)	4.3 ± 1.5 (0.8-7.2)	3.4 ± 1.5 (0.6-6.7)
ER	-2.7 ± 1.1 (-5.9-0.0)	-4.3 ± 1.5 (-7.9--0.8)	-3.4 ± 1.6 (-6.8--0.4)
NEP	-0.7 ± 0.7 (-2.8-1.6)	0.0 ± 0.5 (-1.1-2.0)	0.0 ± 0.2 (-0.8-0.7)

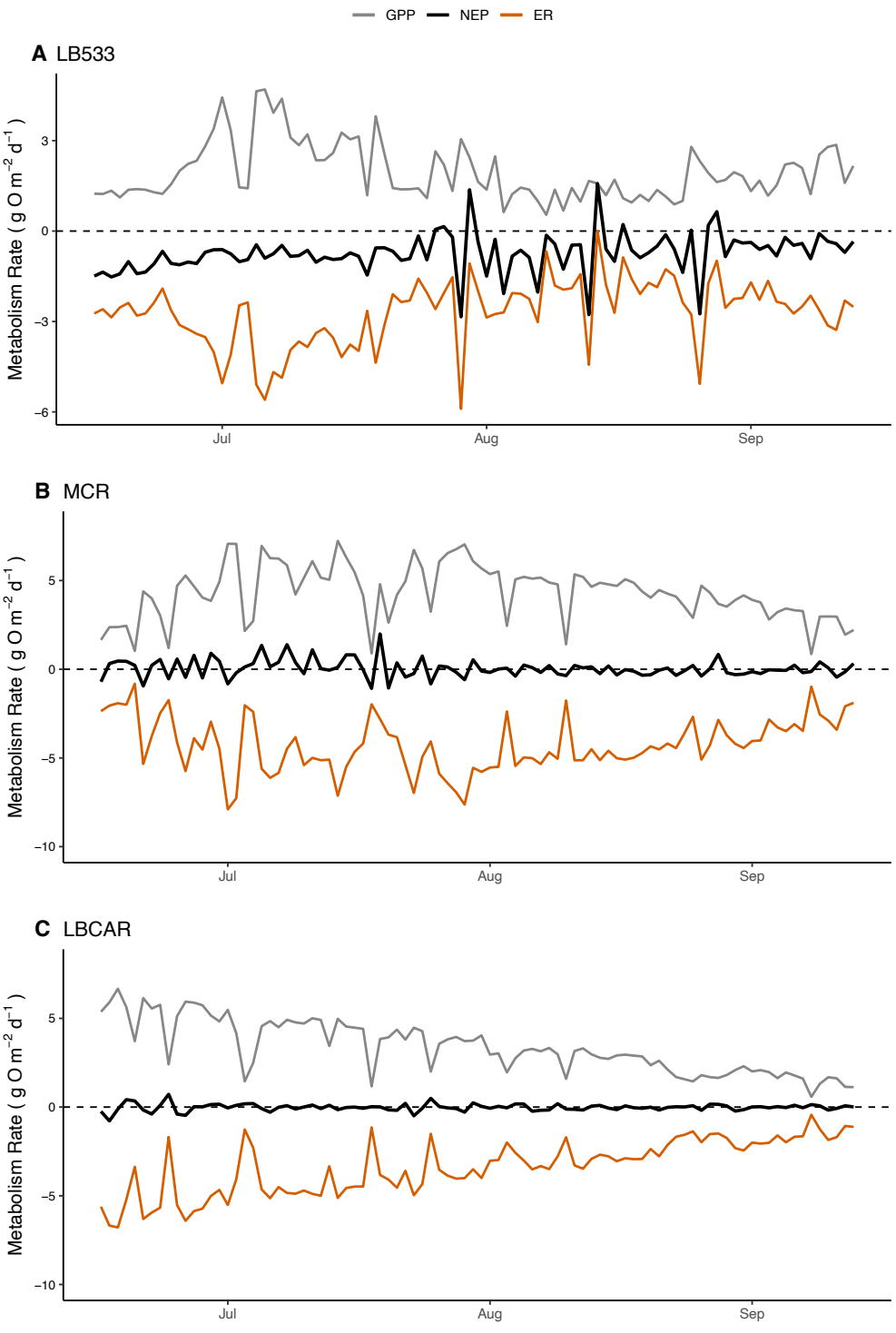

Figure 9. Daily rates of GPP (grey line), ER (orange line), and NEP (black line) for three study sites. Abbreviations defined in text.

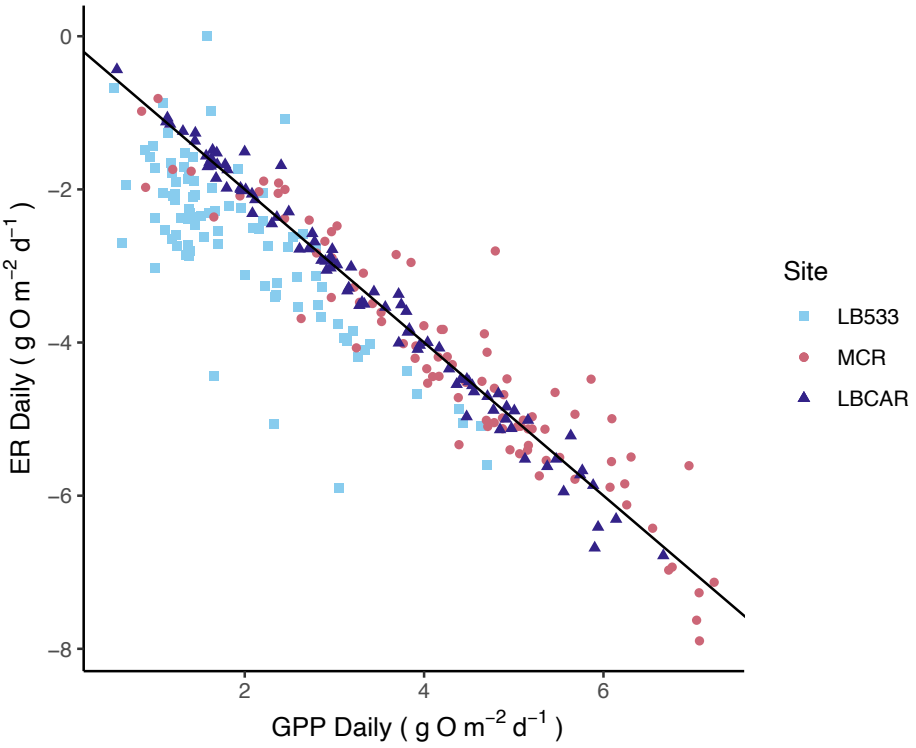

Figure 10. Rates of ER versus GPP for LBR (blue squares), MCR (red points), and LBCAR (purple triangles). The black line denotes where rates of ER (negative) equal GPP.

2.3.6. Cumulative NEP and F_{CO2}

The three sites had variable cumulative NEP (Fig. 11) and F_{CO2} (Fig. 12), with each site having distinct patterns. The final cumulative sum for NEP was -66.53, 4.38, and -1.78 g O_2 m^{-2} for LB533, MCR, and LBCAR, respectively. LB533 had the lowest cumulative NEP of -66.5 g O_2 m^{-2}, while MCR had the greatest of 8.3 g O_2 m^{-2}. LB533 was heterotrophic for the whole year, with an exponential trend towards negative NEP. Conversely, MCR had a positive trend beginning in July until mid-July, where it slowly began to decline, but was still autotrophic (Fig. 11). The cumulative NEP for LBCAR was mainly slightly heterotrophic, with a slight decline throughout the year.

There was a distinct difference in trends of cumulative F_{CO2} between LBR and MCR. The cumulative F_{CO2} for LBR was 449.3 $\pm$ 187.1 with the max of 705.5 g C m^{-2}. The cumulative F_{CO2} for MCR was 62.4 $\pm$ 116.9 and max of 236.3 g C m^{-2}. There was a positive exponential trend for F_{CO2} at LBR, while MCR had a negative F_{CO2} until mid-July where it then began to increase, becoming positive mid-August, where there was a large increase in F_{CO2} from the end of August until September (Fig. 12).

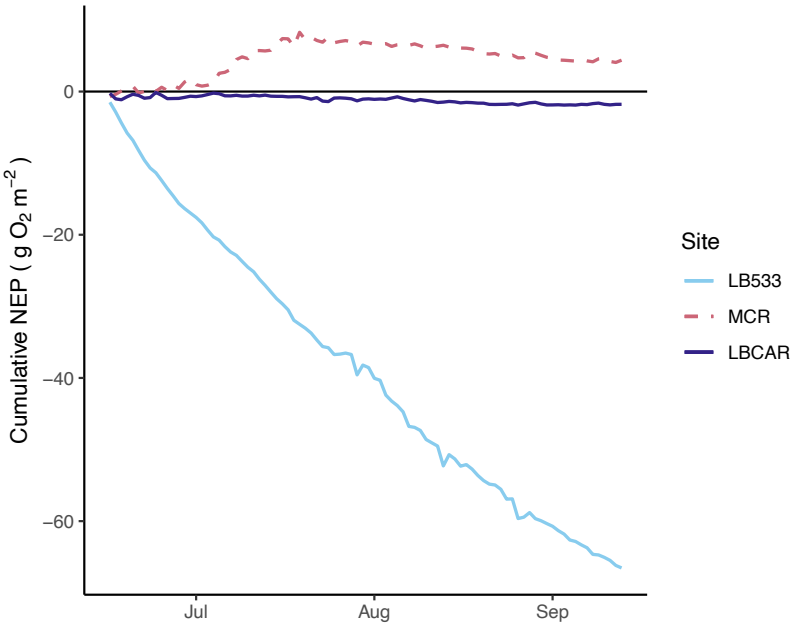

Figure 11. The cumulative sum of daily rates of NEP for LBR (light blue line), MCR (pink dashed line), and LBCAR (purple line) over the sampling period. The horizontal black line is NEP = 0.

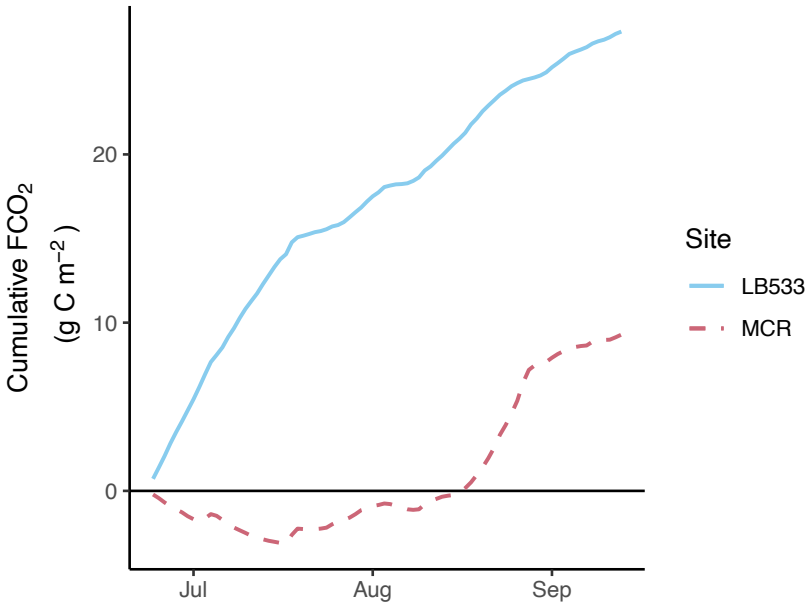

Figure 12. The cumulative sum of daily F_{CO2} rates for LBR (blue line) and MCR (pink dashed line) over the sampling period.

2.3.7. Linking daily rates of high-frequency emissions and NEP

While I observed differences in trends from one day to the next between both sites, there were no significant differences between the two sites in terms of the relationships between the daily rates of F_{CO2} and NEP (Fig. 13, ANCOVA: $F = 0.138$, p = 0.71). Additionally, within each site, there was no significant relationship between rates of F_{CO2} and NEP. A weak, non-significant relationship between F_{CO2} and NEP existed, as suggested by Pearson correlation for both MCR ($r = -0.14$, $p = 0.20$) and LBR ($r = -0.17$, $p = 0.12$). MCR had a greater proportion of data with negative F_{CO2} and positive NEP, signifying more in gassing of CO_2 into the river and net autotrophy, compared to LBR.

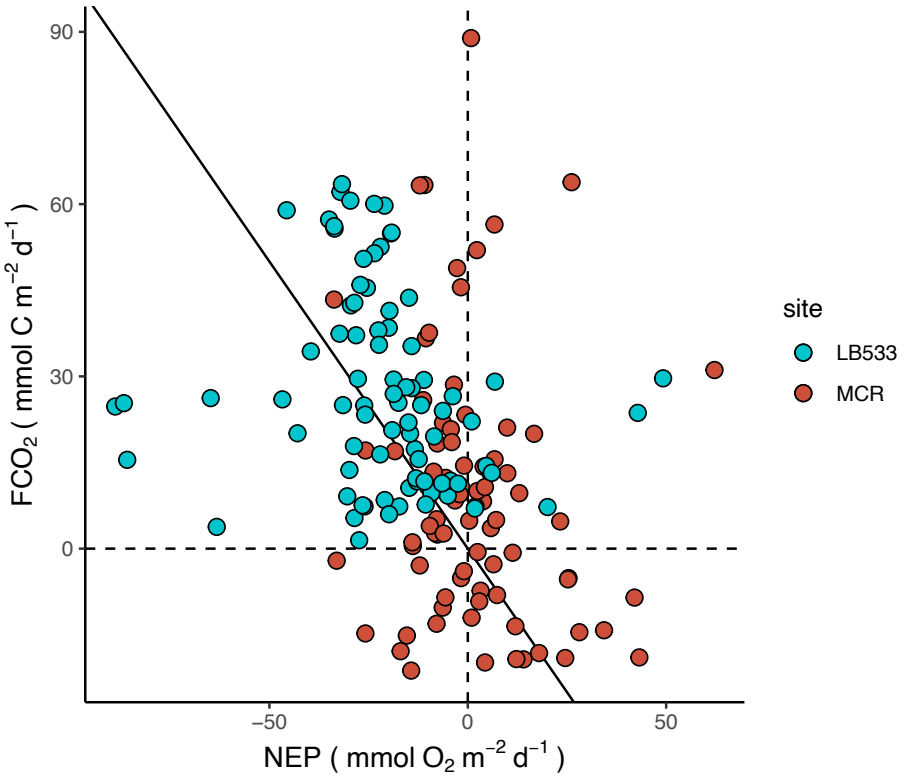

Figure 13. Relationship between daily rates of NEP and emissions of CO_2 for LBR (blue points) and MCR (red points). The solid black line represents the -1:1 relationship.

2.4. Discussion

The C cycle of Canadian rivers in agricultural landscapes, particularly those dominated by irrigation, is not well defined. Multiple lines of evidence indicate that river metabolism and C emissions in the Little Bow River network is weakly influenced by terrestrial C inputs, at least during drought years in 2021 - 2022. First, I used a combination of basin-wide surveys and high-frequency measurements at select locations, which revealed that CO_2 concentrations were low (520 to 1174 μatm; Table 1) compared to the global average river *p*CO2 of 2400 uatm (Lauerwauld et al., 2015). Consequently, the rates of emissions were also generally low in the river network. Second, the average rates of NEP from spring to fall were near zero in two of the three sites that I monitored for metabolism (MCR and LBCAR), and moderately heterotrophic at the other, more upstream site (LB533; Table 2, Fig. 11). These values of NEP were more balanced than previously reported for many rivers that are typically more heterotrophic (e.g., Bernot et al. 2010; Demars et al., 2011). Third, the bioavailability of DOC decreased from upstream to downstream, particularly below the TVR (Fig. 6). While the percent removal was generally high compared to values in other studies (discussed below), the total DOC mineralized was a small quantity. My work also presents new, network-scale patterns of river C cycling for agricultural regions, which expands on previous studies conducted at single locations in the Oldman River watershed (e.g., Zhou et al. 2024). I document a shift in C cycling patterns from headwaters to the lower river, by showing a close coupling of production and respiration in much of the network (Fig. 10), leading to lower bioavailability of DOM (Fig. 6a), and ultimately, elevated pH and lower CO_2 emissions downstream (Fig. 5d, 7c). Whole network perspectives like this are needed, especially in agriculturally dominated systems, as they are underrepresented in the literature (Webb et al., 2019).

Taken together, my thesis provides an improved understanding of riverine C cycling in drought-stressed agricultural landscapes.

2.4.1 The Little Bow River network is a weak CO_2 emitter

Overall, emissions in the Little Bow River network are relatively low due to a combination of low CO_2 availability to fuel outgassing, plus physical conditions that lead to intermediate gas transfer values. Globally, F_{CO2} is highly variable and depends on C availability and the sufficient supply of CO_2 to sustain emissions; even where river turbulence is high, emissions rates can be low if CO_2 pools are depleted (Rocher-Ros et al., 2019). In line with these expectations, I observed low and decreasing rates of emissions from up to downstream, from 68.6 to 13 mmol C m^{-2} d^{-1} from LBCAN to LBCAR sampling sites. High-frequency estimates of C emissions generally agreed with the low-frequency data; the cumulative flux at LB533 was greater than at MCR (Fig. 12), in line with higher median values of F_{CO2} in the low-frequency dataset for both sites (Fig. 7c; $p < 0.05$). High-frequency F_{CO2} values were also low at both sites and even negative, or in-gassing, on many days for MCR. It was likely that the low pCO_2 values (520 to 1174 uatm; Table 1) were driving the patterns of F_{CO2}, since they were much lower than the global mean river pCO_2 of 2400 uatm (Lauerwauld et al., 2015). At the same time, gas transfer velocities were not anomalously low. The k_{600} decreased from upstream to downstream for most of the river network until the TVR, where it increased to intermediate values at the TVRD site immediately below the reservoir (Fig. 7b). Yet overall, k_{600} values were all below 12.0 and averaged 2.2 to 7.9 m d^{-1} (Table 1). These values are in line with averages reported for global rivers (5.7 m d^{-1}; Raymond et al. 2013). As all the sites I sampled have flat topography (i.e., low river channel slopes) and low discharge rates, these values of k_{600} are much lower than those reported for steeper terrain (e.g., mean k_{600} values of 464 m d^{-1} for Alpine streams (Ulseth et al., 2019). In summary, C source limitation appears to

be the driving factor that restricted rates of F_{CO2} in the river network, at least during the drought period when sampling was conducted.

The presence of the reservoir along the Little Bow River (TVR; Fig. 3) appeared to have little effect on downstream CO_2 emissions. This was somewhat surprising because reservoirs are widely recognized as hotspots for OM mineralization (Maavara et al., 2017). However, some studies have found that impoundment may decrease downstream pCO_2 due to high productivity in the reservoir and an increase in pH (Ran et al., 2015; Chan et al. 2023; Yan et al., 2022). Other studies have made opposite observations, as highly stratified reservoirs increase the concentration of hypolimnetic CO_2 and, therefore, when bottom water is discharged downstream, it has higher CO_2 content to support greater emissions rates (Abril et al., 2015; Calamita et al., 2021). In our case, the TVR appears not to be strongly stratified during ice-free months of sampling (data not shown) or in earlier years (Sosiak, 2011). It is, therefore, likely that much of the CO_2 produced in the reservoir is emitted to the atmosphere on site. While the TVR is a bottom-discharge reservoir (Sosiak 2011), the lack of hypolimnetic CO_2 buildup may be the main reason why it does not export CO_2-rich waters and is not enhancing downstream emissions. Follow up research is needed to better integrate the emissions from the TVR with the rest of the river network.

2.4.2 Metabolism in the Little Bow River and Mosquito Creek

In recent decades, there have been many advancements in understanding how river metabolism impacts not only regional but global C cycling and budgets (e.g., Battin et al., 2009; Hotchkiss et al., 2015; Bernhardt et al., 2022). However, there is a lack of research in western Canadian rivers on the drivers and controls of metabolism, and implications for river C cycling. Here, I found that modelled rates of metabolism in the Little Bow River network, on average, were higher for GPP but lower for ER (mean GPP from 2.0 to 4.3; mean ER from -2.7 to -4.3; Table 2) than median rates reported by Hall and Hotchkiss (2017) for global rivers (median GPP = 1.6 g O_2 m^{-2} d^{-1} ;

median ER = -4.7 g O_2 m^{-2} d^{-1}). For agricultural regions, more specifically, my results agree with some but not other past studies. For streams in Indiana, U.S.A., Griffiths et al. (2013) reported similar rates of GPP (mean = 4.6 g O_2 m^{-2} d^{-1}), but much greater rates of ER (mean = -10.5 g O_2 m^{-2} d^{-1}) than I observed. Consequently, these streams were more heterotrophic than in my study. On the other hand, the mean rates I report are similar to those from streams in Idaho, U.S.A. (Honious et al., 2021) that had mean GPP (2.1 g O_2 m^{-2} d^{-1}) and ER (-2.6 g O_2 m^{-2} d^{-1}) more in balance and NEP closer to zero. Broader surveys of agricultural streams (Bernot et al., 2010) have shown that GPP can range widely from 0.1 to 16.2 g O_2 m^{-2} d^{-1}, and that rates of ER typically exceed GPP, and span -0.4 to -23.1 g O_2 m^{-2} d^{-1}. Yet that survey was based on small streams in the U.S., and broader assessments in other parts of the world showed my observed rates were similar to low metabolic rates for rivers in the Ebro basin in Spain (Aristi et al., 2014) and agricultural streams on the Swedish Island of Oland in the southern Baltic Sea (Alnoee et al., 2015). A past study using a comparable free water approach in the mainstem of the Oldman River showed summertime GPP also ranged from ~3.5 to 8 g O_2 m^{-2} d^{-1} (Brinkmann & Rasmussen 2012). This indicates that while the Little Bow River network is a relatively productive habitat compared to most global rivers, the rates are on the low end (but not outliers) for rivers in agricultural zones or the broader Oldman River network.

Variations in food web functioning among rivers and sites are complex, and the underlying drivers can be hard to determine. By monitoring three different sites along two separate rivers, I identified a range of metabolic properties through the river network, with one site being heterotrophic, one being weakly autotrophic, and another in near metabolic balance (Fig. 11). This was surprising, given the close geographic proximity of the sites. I attribute these differences to unique combinations of environmental drivers dominating at each site (Fig. 14). Bernhardt et al.

(2018) proposed a framework for comparing metabolic patterns between rivers or years. They suggest that deviation from the -1:1 ER:GPP line toward heterotrophy could be due to greater DOC and nutrient inputs and warming, while a compression towards the -1:1 line is mainly driven by hydrology (increased flows and scouring of the riverbed). Given that average water temperatures were quite consistent between sites (Table 1; Appendix D2), and light availability was also similar (i.e., no tree coverage and similar water clarity), it is likely that these factors were less important in driving between-site differences in net metabolism (Fig. 14).

Instead, heterotrophy at the LB533 site was likely due to a combination of higher discharge and variable depth limiting GPP, and elevated bioavailable OM inputs supporting ER (Fig. 14). Although LB533 had the lowest rates of GPP and ER, it had the largest and most negative rates of NEP (Fig. 9, Fig. 11) and remained heterotrophic for the entire sampling period. This agrees with the elevated rates of F_{CO2} at this location (Fig. 12). The relationship between ER and GPP was shifted downward towards greater rates of ER (Fig 10). This could be due to external (i.e., loaded upstream) inputs of OM sustaining greater rates of ER and heterotrophic respiration. Accordingly, of the three sites, the fraction of DOC that was bioavailable to microbes was greatest at LB533 (Fig. 6b). LBR receives effluent from the outflow of Frank Lake, which receives effluent from both the town of High River and the Cargill meat processing plant that can then be processed by Frank Lake. While the connection between Frank Lake outflow and the Little Bow River was absent during most of the drought period (Zhou et al. 2023), historical loading and buildup of nutrients and OM in the watershed may support this elevated BDOC. At the same time, higher mean discharge at LB533 could be a factor driving the low rates of GPP due to changes in water depth (Appendix D1), sediment load, and impacts on algal communities via scouring of attached biomass (Bernhardt et al., 2018).

At the MCR site, the balanced to autotrophic NEP that I observed was likely driven by stable flow regimes and water depth, despite an abundance of relatively bioavailable DOM (Fig. 14). MCR receives effluent from the upstream town of Nanton that is discharged directly into the river. This may explain the elevated proportion of BDOC (Fig. 6b) that may sustain elevated ER (Fig. 14) (Arroita et al. 2014). Yet, MCR had the lowest and most stable rates of discharge through time (Fig. 4), with somewhat variable depth (Appendix D1) (Fig. 14). Bernhardt et al. (2022) found that more stable flow regimes increased the median GPP values in streams three times greater than rates in ecosystems with variable flow regimes. In line with this, MCR had the highest average rates of GPP and ER (Table 2), but NEP was slightly autotrophic (Fig. 11). Furthermore, the relationship between ER and GPP was tightly coupled near -1:1 (Fig. 10). Overall, it appears that the stable hydrology in this reach may be the ultimate control of food web metabolism during the current drought, with drought-driven shifts to autotrophy being common in other regions (Hosen et al., 2019).

Finally, conditions at the LBCAR site differed from those upstream, leading to near-balanced NEP (Fig. 14). While LBCAR is an integration of water masses from both upstream sites receiving effluent, the upstream processing of OM and nutrients may attenuate this effect. While the low-frequency sampling indicated that there was an increase in DOC content from headwaters to downstream (Table 1), the actual bioavailability decreased (Fig. 6b, based on %BDOC as a relative indicator) to extremely low levels at LBCAR, thereby limiting the capacity for microbes to consume OM and enhance ER (Fig. 14). In addition, the TVR may be impacting downstream metabolism at LBCAR, caused by water release, which led to intermediate variability in channel depth (Appendix D1) and discharge (Fig. 4) (Fig. 14). Multiple studies have found that GPP can increase in rivers below reservoirs and impoundments (Hunt et al., 2012; Chowanski et al., 2020).

In the case of LBCAR, the GPP is higher than one of the two sites, so exploring metabolism further downstream may provide better insight into how C cycling is being impacted by the reservoir in more detail. Upstream dams also increased GPP and ER in Mediterranean rivers, as there was less hydrologic variability, and pelagic GPP contributing to downstream GPP, with NEP ranging from -2.52 to -0.36 g O_2 m^{-2} d^{-1} (Aristi et al., 2014).

Ultimately, the availability of light, nutrients, and discharge are driving factors of river metabolism patterns around the world (Battin et al., 2023). Here in the Little Bow River, which is a heavily regulated network, the impacts of human alteration on flow regimes and nutrient and OM availability may be impacting metabolic rates in major ways throughout the river network that manifest differently through space and time. While a deeper investigation of temporal metabolic patterns is beyond the scope of my thesis, it could provide further insight into the functioning of the river food web.

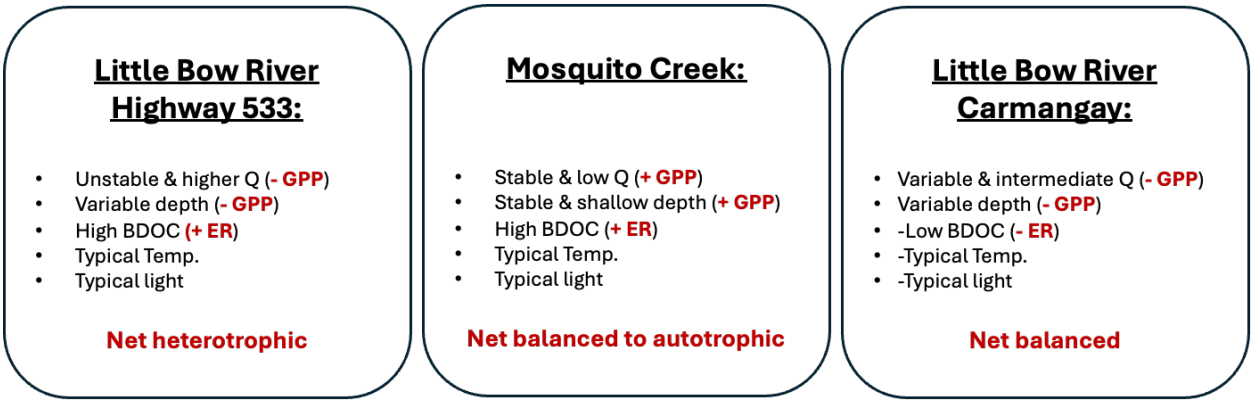

Figure 14. A summary of the different environmental controls of site-specific metabolism at my three monitoring locations. The net metabolic balances indicated in red are determined by both averaged NEP rates (Table 2) and cumulative NEP calculated in Figure 11. The key directional influences of parameters on either GPP or ER are summarized in parentheses in red bolded text.

2.4.3 Connection between NEP and CO_2 emissions

Rivers contribute disproportionately to the annual budget of atmospheric CO_2 emissions (Cole et al., 2007; Raymond et al., 2013), but the proportion of emissions attributed to internal river metabolism versus external CO_2 loading is poorly constrained (Hotchkiss et al., 2015). By pairing sensor-based measurements of NEP with F_{CO2} (Fig. 13), I found that the coupling of metabolism and emissions was relatively weak, at least on averaged daily timescales. Points measured for MCR fell in all four quadrants (as delineated by both positive and negative NEP and F_{CO2} values), and points spanned both sides of the -1:1 line with low correlative strength (Fig. 13). While points for LB533 fell only in two quadrants (positive F_{CO2}, and both positive and negative NEP), the values also spanned the -1:1 line and had equally weak correlation (Fig. 13). This weak coupling that I observed is not unprecedented. Reed et al. (2021) found that during snowmelt, there was a moderate correlation between NEP and F_{CO2}, driven by allochthonous C inputs that stimulated both ER and F_{CO2}. However, they found no correlation during the non-snow melt period, as was the case for both MCR and LBR. At the same time, Solano et al. (2023) found rates of heterotrophic NEP often exceeded F_{CO2} outgassing rates, possibly due to the low turbulence and low evasion rates that led to lateral CO_2 export instead of direct emissions on site. As their gas transfer velocity rates were consistent with my measurements (~3 to 9 m d^{-1}), this mechanism may partly explain the decoupling of NEP and F_{CO2} here. At the same time, DIC buffering likely decoupled NEP and F_{CO2}. There were large diel patterns of pCO_2 and pH at both of my sites (Fig. 8), indicating that while metabolism drives DIC dynamics at sub-hourly scales, the addition and removal of CO_2 shifts the balance of bicarbonate (HCO_3^-) and carbonate (CO_3^{2-}) in ways that buffer CO_2 availability and decouple F_{CO2} and NEP (Stets et al. 2017), especially in alkaline waters like our study sites (data not shown). This can ultimately lead to excess CO_2 during periods of intense photosynthesis, sustaining greater emissions than predicted by NEP (Stets et al. 2017). Overall,

the mechanisms underlying the coupling of these two rate measurements are complex and should be fully characterized in the future.

2.4.4. In stream processing and implications for the riverine C pool

Overall, the C pool in the Little Bow River network was dominated by DIC (~5 to 30 times greater than DOC content; Fig. 5c). This is consistent with general expectations for other agricultural rivers in North America (Tank et al. 2018), yet this balance was not static. While low pCO_2 and high pH values were relatively stable throughout the network, the ratio of DIC:DOC decreased moving downstream. DIC concentrations were relatively stable, but those of DOC increased downstream (Fig. 5). The decrease in the DIC:DOC ratio may suggest an important role in the system for DOC production by autotrophs via GPP. TVRD and LBCAR had the highest Chl *a* concentrations (Table 1), indicating that suspended plankton could have been a greater downstream source of autochthonous DOC. The temperature was greatest at LBCAR, the furthest downstream site (Table 1), and this could have increased the internal processing of C and production of DOC. However, the balanced values of NEP (on average; Table 2) do not necessarily support these hypotheses. Another potential factor driving the shift in DIC:DOC ratios could be an accumulation of less bioavailable DOC as water masses moved downstream. In line with this hypothesis, I observed a shift from high to low BDOC values, especially after the TVR (Fig. 6). This may be attributed to the higher water residence time in the TVR, allowing for greater processing of the DOC pool, leaving more recalcitrant or less bioavailable DOC that was released downstream. Overall, C dynamics in river systems can be highly variable and unpredictable, demonstrating the need for more holistic studies that combine multiple C parameters for understudied regions of Canada and the world.

2.4.5 Limitations

My study provides new insights into river C cycling and metabolism owing to the combination of multiple methods (incubations, routine chemical analysis, and sensor deployment) applied to sampling frequencies that span sub-hourly to annual timeframes. However, there are still some uncertainties about C cycling in my study sites, and in southern Albertan rivers more broadly. One limitation is for two (LBCAN and LBUP) of the seven sites; the gauging station was not directly at the site of water sampling, and this could have impacted the accuracy of my calculations for the low-frequency datasets, especially for k_{600} calculations and, therefore, rates of CO_2 emissions (F_{CO2}). There are multiple variables that are needed in calculating k_{600}, with depth driving better k_{600} models (Raymond et al, 2012), highlighting the importance of having accurate depth measurements.

Second, the sampling time of my routine site visits and BDOC incubations also impacts my interpretations of ecosystem functioning since it does not capture the effects of diel shifts in metabolism on several of the chemical variables, particularly gas content (e.g., CO_2 or DO concentrations), or changes in bioavailability seasonally. All my water sampling occurred during the day. Therefore, I only captured C dynamics when rates of GPP were high and pCO_2 was lowest (Fig. 7). The C dynamics during the night would shift as the ecosystem becomes dominated by ER (de Montety et al., 2011). Despite this, mean pCO_2 values for high-frequency measurements that do integrate diel changes (Fig. 8) align with low-frequency measurements (Fig. 7). To dive deeper into the patterns and controls of whole network C cycling, sensors measuring DO and pH could be deployed more extensively along the river continuum to record high-frequency conditions and determine how changes in metabolism impact CO_2 cycling and emissions throughout the network.

Third, the frequency of sampling could be increased in future work by conducting multiple surveys each month as well as performing multiyear analyses that capture shifting hydroclimatic

conditions. Future studies could perform multiple BDOC incubations throughout the year to determine how bioavailability changes seasonally (e.g., Zhou et al. 2024), and how this influences not only river metabolism but C cycling. As my study took place during an extended, multi-year drought (Zhou et al. 2023), examining C cycling during a wet year with greater habitat connectivity and higher flow rates would enable the comparison between different hydroclimatic conditions and how this influences river C cycling. For instance, Val et al. (2016) tracked river metabolic patterns over multiple years and hydroclimatic conditions and found that during increasing flow periods, GPP decreased in response to decreased light availability and increased turbidity. They found that in subsequent drought periods, lower flow rates enhanced GPP but not ER, but then later flooding events affected ER in different ways. Follow-up research in the Little Bow River could follow a longer-term sampling framework like that of Val et al. (2016), demonstrating that our interpretation of long-term metabolic functioning and C cycling requires sampling over different hydrologic conditions.

Fourth, my study overlooked methods that identify the structure of the food web and potential shifts along the hydrologic continuum. This would provide some insight into the potential controls on river metabolism throughout the network. While I sampled suspended Chl *a* content, I did not include samples of plant or animal communities, nor estimates of attached biomass, which is extensive at some sites (APPENDIX A3;A6). This attached algal biomass could enhance GPP independent of our measurements of suspended Chl *a*. Further, to understand C processing patterns in subsurface habitats, examining the microbial communities in the streambed and their links to C cycling would provide a unique perspective on river functioning.

Chapter 3. CONCLUSIONS

Rivers play an important role in the global C cycle by transporting C from land to sea (Fig. 1). Once viewed only as a pipe for C to the ocean, they are now understood to also be important sites for the active processing of C (Cole et al., 2007). Yet region-specific information on river C cycling is patchy. In western Canada, the patterns and controls of river metabolism and C cycling are understudied and not well defined. My study explored the complex C cycling and metabolic processes in a river network that is heavily impacted by agricultural and urban activities. The first part of my study explored spatial patterns of DIC and DOC, pCO_2, and CO_2 emissions. Furthermore, I used a 28-day BDOC incubation experiment to determine how the bioavailability of the DOC pool shifts within the system from upstream to downstream habitats. I had seven sites along two different rivers, with two sites downstream of a reservoir, capturing a large gradient of disturbances and physicochemical conditions throughout the watershed. Ultimately, I showed that the C pool shifts from upstream to downstream with decreasing trends in the ratios of DIC:DOC, decreasing pCO_2 and FCO_2, and decreasing absolute and proportional BDOC availability. This trend may be due to each site's specific geomorphology, differing discharge rates, and metabolic processing. I found an increasing trend in both DOC and pH, underscoring the importance of how upstream processing of C impacts the processes occurring in downstream reaches. I found that the TVR reduced the amount of BDOC available for downstream sites, signifying the importance of reservoirs and impoundments in river networks as sites of control on river network C cycling.

Secondly, I modelled river metabolism for three of the seven sites (LB533, MCR, and LBCAR). The rates of metabolism were on the low side for agricultural rivers and streams (Bernot et al., 2010) but higher than mean values for rivers globally (Hall and Hotchkiss, 2017), indicating that the LBR watershed is relatively productive and in line with observations in the larger Oldman

River (Brinkmann & Rasmussen 2012). The magnitude of metabolic rates differed among the sites, and I found more balanced metabolic rates and C processing at MCR and LBCAR than at LB533 (which was heterotrophic). I attributed these differences to variable discharge rates and depth and the bioavailability of C at each site. The unique temporal patterns in hydrologic conditions across the sites were likely due to water withdrawal for irrigation and release from reservoirs that may influence the local factors controlling river metabolism.

Finally, I used a combination of high-frequency pH measurements to determine sub-daily patterns of CO_2 emissions and support metabolism models. Using both, I could determine the relationship between river metabolism and CO_2 emissions at two different sites. I found that there was a weak, inverse, non-significant relationship between FCO_2 and NEP for both sites. Although there was little correlation between FCO_2 and NEP, both the cumulative NEP and FCO_2 patterns from spring to fall agreed and showed distinct trends between LB533 and MCR. LB533 was heterotrophic for the whole year while MCR was autotrophic until mid-August, where then cumulative NEP decreased, and *F*CO2 increased, coinciding with increased discharge and mean depth. The differences in C cycling between these two sites demonstrate how understanding the changes in hydrology and river physicochemical properties are fundamental to predicting patterns of river metabolism and C pool shifts. Clearly, human interventions that change the hydrology of the Little Bow River network exert important overall controls on river functioning.

This was one of the first studies that combined high-frequency and low-frequency CO_2 fluxes, BDOC incubations, and river metabolism measurements in the agricultural landscapes of western Canada, enabling me to provide new insights into how C is being cycled throughout the ULB watershed. My findings add to the literature investigating river functioning at the larger, network scale.

REFERENCES

Åberg, J., & Wallin, M. (2014). Evaluating a fast headspace method for measuring DIC and subsequent calculation of pCO2 in freshwater systems. *Inland Waters*, *4*(2), 157–166. https://doi.org/10.5268/IW-4.2.694

Abril, G., Bouillon, S., Darchambeau, F., Teodoru, C. R., Marwick, T. R., Tamooh, F., Ochieng Omengo, F., Geeraert, N., Deirmendjian, L., Polsenaere, P., & Borges, A. V. (2015). Technical Note: Large overestimation of pCO_2 calculated from pH and alkalinity in acidic, organic-rich freshwaters. *Biogeosciences*, *12*(1), 67–78. https://doi.org/10.5194/bg-12-67-2015

Abril, G., Martinez, J.-M., Artigas, L. F., Moreira-Turcq, P., Benedetti, M. F., Vidal, L., Meziane, T., Kim, J.-H., Bernardes, M. C., Savoye, N., Deborde, J., Souza, E. L., Albéric, P., Landim De Souza, M. F., & Roland, F. (2014). Amazon River carbon dioxide outgassing fuelled by wetlands. *Nature*, *505*(7483), 395–398. https://doi.org/10.1038/nature12797

Alnoee, A. B., Riis, T., Andersen, M. R., Baattrup-Pedersen, A., & Sand-Jensen, K. (2015). Whole-stream metabolism in nutrient-poor calcareous streams on Öland, Sweden. *Aquatic Sciences*, *77*(2), 207–219. https://doi.org/10.1007/s00027-014-0380-5

Appling, A. P., Hall Jr., R. O., Yackulic, C. B., & Arroita, M. (2018a). Overcoming Equifinality: Leveraging Long Time Series for Stream Metabolism Estimation. *Journal of Geophysical Research: Biogeosciences*, *123*(2), 624–645. https://doi.org/10.1002/2017JG004140

Appling, A. P., Read, J. S., Winslow, L. A., Arroita, M., Bernhardt, E. S., Griffiths, N. A., Hall, R. O., Harvey, J. W., Heffernan, J. B., Stanley, E. H., Stets, E. G., & Yackulic, C. B. (2018b). The metabolic regimes of 356 rivers in the United States. *Scientific Data*, *5*(1), Article 1. https://doi.org/10.1038/sdata.2018.292

Aristi, I., Arroita, M., Larrañaga, A., Ponsatí, L., Sabater, S., von Schiller, D., Elosegi, A., & Acuña, V. (2014). Flow regulation by dams affects ecosystem metabolism in Mediterranean rivers. *Freshwater Biology*, *59*(9), 1816–1829. https://doi.org/10.1111/fwb.12385

Arroita, M., Elosegi, A., & Hall Jr., R. O. (2019). Twenty years of daily metabolism show riverine recovery following sewage abatement. *Limnology and Oceanography*, *64*(S1), S77–S92. https://doi.org/10.1002/lno.11053

Aufdenkampe, A. K., Mayorga, E., Raymond, P. A., Melack, J. M., Doney, S. C., Alin, S. R., Aalto, R. E., & Yoo, K. (2011). Riverine coupling of biogeochemical cycles between land, oceans, and atmosphere. *Frontiers in Ecology and the Environment*, *9*(1), 53–60. https://doi.org/10.1890/100014

Battin, T. J., Lauerwald, R., Bernhardt, E. S., Bertuzzo, E., Gener, L. G., Hall, R. O., Hotchkiss, E. R., Maavara, T., Pavelsky, T. M., Ran, L., Raymond, P., Rosentreter, J. A., & Regnier, P. (2023).

River ecosystem metabolism and carbon biogeochemistry in a changing world. *Nature*, *613*(7944), Article 7944. https://doi.org/10.1038/s41586-022-05500-8

Battin, T., Kaplan, L., Findlay, S., Hopkinson, C., Martí, E., Packman, A., Newbold, D., & Sabater, F. (2009). Biophysical controls on organic carbon fluxes in fluvial networks. *Nature Geoscience*, *1*, 95–100. https://doi.org/10.1038/ngeo101

Bauer, J. E., Cai, W.-J., Raymond, P. A., Bianchi, T. S., Hopkinson, C. S., & Regnier, P. A. G. (2013). The changing carbon cycle of the coastal ocean. *Nature*, *504*(7478), Article 7478. https://doi.org/10.1038/nature12857

Bernhardt, E. S., Heffernan, J. B., Grimm, N. B., Stanley, E. H., Harvey, J. W., Arroita, M., Appling, A. P., Cohen, M. J., McDowell, W. H., Hall Jr., R. O., Read, J. S., Roberts, B. J., Stets, E. G., & Yackulic, C. B. (2018). The metabolic regimes of flowing waters. *Limnology and Oceanography*, *63*(S1), S99–S118. https://doi.org/10.1002/lno.10726

Bernhardt, E. S., Savoy, P., Vlah, M. J., Appling, A. P., Koenig, L. E., Hall, R. O., Arroita, M., Blaszczak, J. R., Carter, A. M., Cohen, M., Harvey, J. W., Heffernan, J. B., Helton, A. M., Hosen, J. D., Kirk, L., McDowell, W. H., Stanley, E. H., Yackulic, C. B., & Grimm, N. B. (2022). Light and flow regimes regulate the metabolism of rivers. *Proceedings of the National Academy of Sciences*, *119*(8), e2121976119. https://doi.org/10.1073/pnas.2121976119

Bernot, M. J., Sobota, D. J., Hall Jr, R. O., Mulholland, P. J., Dodds, W. K., Webster, J. R., Tank, J. L., Ashkenas, L. R., Cooper, L. W., Dahm, C. N., Gregory, S. V., Grimm, N. B., Hamilton, S. K., Johnson, S. L., Mcdowell, W. H., Meyer, J. L., Peterson, B., Poole, G. C., Valett, H. M., … Wilson, K. (2010). Inter-regional comparison of land-use effects on stream metabolism. *Freshwater Biology*, *55*(9), 1874–1890. https://doi.org/10.1111/j.1365-2427.2010.02422.x

Bogard, M. J., Gunawardana, P. V. S. L., Soued, C., Kalyn Bogard, H. J., Smits, K. M., & Flanagan, L. B. (2023). Heterotrophic aquatic metabolism and sustained carbon dioxide emissions in a mineral-soil wetland restored with treated effluent. *Science of The Total Environment*, *884*, 163584. https://doi.org/10.1016/j.scitotenv.2023.163584

Bogard, M. J., Vogt, R. J., Hayes, N. M., & Leavitt, P. R. (2020). Unabated Nitrogen Pollution Favors Growth of Toxic Cyanobacteria over Chlorophytes in Most Hypereutrophic Lakes. *Environmental Science & Technology*, *54*(6), 3219–3227. https://doi.org/10.1021/acs.est.9b06299

Brinkmann, L., & Rasmussen, J. B. (2010). High levels of mercury in biota of a new Prairie irrigation reservoir with a simplified food web in Southern Alberta, Canada. *Hydrobiologia*, *641*(1), 11–21. https://doi.org/10.1007/s10750-009-0050-0

Butman, D. E., Wilson, H. F., Barnes, R. T., Xenopoulos, M. A., & Raymond, P. A. (2015). Increased mobilization of aged carbon to rivers by human disturbance. *Nature Geoscience*, *8*(2), 112–116. https://doi.org/10.1038/ngeo2322

Calamita, E., Siviglia, A., Gettel, G. M., Franca, M. J., Winton, R. S., Teodoru, C. R., Schmid, M., & Wehrli, B. (2021). Unaccounted CO2 leaks downstream of a large tropical hydroelectric reservoir. *Proceedings of the National Academy of Sciences*, *118*(25), e2026004118. https://doi.org/10.1073/pnas.2026004118

Chan, C. N., Bogard, M. J., Ma, F. C., Ip, Y. C., Liu, B., Chen, S., & Ran, L. (2023). CO2 dynamics in a small and old subtropical reservoir in East Asia: Environmental controls driving seasonal and spatial variability. *Science of The Total Environment*, *856*, 159047. https://doi.org/10.1016/j.scitotenv.2022.159047

Chowanski, K., Kunza, L., Hoffman, G., Genzoli, L., & Stickney, E. (2020). River management alters ecosystem metabolism in a large oligotrophic river. *Freshwater Science*, *39*(3), 534–548. https://doi.org/10.1086/710082

Cole, J. J., Prairie, Y. T., Caraco, N. F., McDowell, W. H., Tranvik, L. J., Striegl, R. G., Duarte, C. M., Kortelainen, P., Downing, J. A., Middelburg, J. J., & Melack, J. (2007). Plumbing the Global Carbon Cycle: Integrating Inland Waters into the Terrestrial Carbon Budget. *Ecosystems*, *10*(1), 172–185. https://doi.org/10.1007/s10021-006-9013-8

Cory, R. M., & McKnight, D. M. (2005). Fluorescence Spectroscopy Reveals Ubiquitous Presence of Oxidized and Reduced Quinones in Dissolved Organic Matter. *Environmental Science & Technology*, *39*(21), 8142–8149. https://doi.org/10.1021/es0506962

Cory, R. M., Ward, C. P., Crump, B. C., & Kling, G. W. (2014). Sunlight controls water column processing of carbon in arctic fresh waters. *Science*, *345*(6199), 925–928. https://doi.org/10.1126/science.1253119

Cross, W. F., Hood, J. M., Benstead, J. P., Huryn, A. D., Welter, J. R., Gíslason, G. M., & Ólafsson, J. S. (2022). Nutrient enrichment intensifies the effects of warming on metabolic balance of stream ecosystems. *Limnology and Oceanography Letters*, *7*(4), 332–341. https://doi.org/10.1002/lol2.10244

D'Amario, S. C., & Xenopoulos, M. A. (2015). Linking dissolved carbon dioxide to dissolved organic matter quality in streams. *Biogeochemistry*, *126*(1), 99–114. https://doi.org/10.1007/s10533-015-0143-y

de Montety, V., Martin, J. B., Cohen, M. J., Foster, C., & Kurz, M. J. (2011). Influence of diel biogeochemical cycles on carbonate equilibrium in a karst river. *Chemical Geology*, *283*(1), 31–43. https://doi.org/10.1016/j.chemgeo.2010.12.025

de Wit, H. A., Valinia, S., Weyhenmeyer, G. A., Futter, M. N., Kortelainen, P., Austnes, K., Hessen, D. O., Räike, A., Laudon, H., & Vuorenmaa, J. (2016). Current Browning of Surface Waters Will Be Further Promoted by Wetter Climate. *Environmental Science & Technology Letters*, *3*(12), 430–435. https://doi.org/10.1021/acs.estlett.6b00396

Deemer, B. R., Yackulic, C. B., Hall, R. O., Jr, Dodrill, M. J., Kennedy, T. A., Muehlbauer, J. D., Topping, D. J., Voichick, N., & Yard, M. D. (2022). Experimental reductions in subdaily flow fluctuations increased gross primary productivity for 425 river kilometers downstream. *PNAS Nexus*, *1*(3), pgac094. https://doi.org/10.1093/pnasnexus/pgac094

Demars, B. O. l., Russell Manson, J., Ólafsson, J. S., Gíslason, G. M., Gudmundsdóttir, R., Woodward, G., Reiss, J., Pichler, D. E., Rasmussen, J. J., & Friberg, N. (2011). Temperature and the metabolic balance of streams. *Freshwater Biology*, *56*(6), 1106–1121. https://doi.org/10.1111/j.1365-2427.2010.02554.x

Dodds, W. K., & Smith, V. H. (2016). Nitrogen, phosphorus, and eutrophication in streams. *Inland Waters*, *6*(2), 155–164. https://doi.org/10.5268/IW-6.2.909

Drake, T. W., Raymond, P. A., & Spencer, R. G. M. (2018). Terrestrial carbon inputs to inland waters: A current synthesis of estimates and uncertainty. *Limnology and Oceanography Letters*, *3*(3), 132–142. https://doi.org/10.1002/lol2.10055

Duarte, C. M., & Agustí, S. (1998). The CO2 Balance of Unproductive Aquatic Ecosystems. *Science*, *281*(5374), 234–236. https://doi.org/10.1126/science.281.5374.234

Duarte, C., & Prairie, Y. (2005). Prevalence of Heterotrophy and Atmospheric CO2 Emissions from Aquatic Ecosystems. *Ecosystems*, *8*, 862–870. https://doi.org/10.1007/s10021-005-0177-4

Ferreira, V., Elosegi, A., D. Tiegs, S., Von Schiller, D., & Young, R. (2020). Organic Matter Decomposition and Ecosystem Metabolism as Tools to Assess the Functional Integrity of Streams and Rivers–A Systematic Review. *Water*, *12*(12), 3523. https://doi.org/10.3390/w12123523

Fifth Assessment Report—Synthesis Report. (n.d.). Retrieved November 14, 2024, from https://archive.ipcc.ch/report/ar5/syr/

Greimel, F., Schülting, L., Graf, W., Bondar-Kunze, E., Auer, S., Zeiringer, B., & Hauer, C. (2018). Hydropeaking Impacts and Mitigation. In S. Schmutz & J. Sendzimir (Eds.), *Riverine Ecosystem Management* (pp. 91–110). Springer International Publishing. https://doi.org/10.1007/978-3-319-73250-3_5

Griffiths, N. A., Tank, J. L., Royer, T. V., Roley, S. S., Rosi-Marshall, E. J., Whiles, M. R., Beaulieu, J. J., & Johnson, L. T. (2013). Agricultural land use alters the seasonality and magnitude of stream metabolism. *Limnology and Oceanography*, *58*(4), 1513–1529. https://doi.org/10.4319/lo.2013.58.4.1513

Hall Jr., R. O., Yackulic, C. B., Kennedy, T. A., Yard, M. D., Rosi-Marshall, E. J., Voichick, N., & Behn, K. E. (2015). Turbidity, light, temperature, and hydropeaking control primary productivity in the Colorado River, Grand Canyon. *Limnology and Oceanography*, *60*(2), 512–526. https://doi.org/10.1002/lno.10031

Hall, R. O., & Hotchkiss, E. R. (2017). Stream Metabolism. In *Methods in Stream Ecology* (pp. 219–233). Elsevier. https://doi.org/10.1016/B978-0-12-813047-6.00012-7

Hillman, E. J., Bigelow, S. G., Samuelson, G. M., Herzog, P. W., Hurly, T. A., & Rood, S. B. (2016). Increasing River Flow Expands Riparian Habitat: Influences of Flow Augmentation on Channel Form, Riparian Vegetation and Birds Along the Little Bow River, Alberta. *River Research and Applications*, *32*(8), 1687–1697. https://doi.org/10.1002/rra.3018

Honious, S. A. S., Hale, R. L., Guilinger, J. J., Crosby, B. T., & Baxter, C. V. (2022). Turbidity Structures the Controls of Ecosystem Metabolism and Associated Metabolic Process Domains Along a 75-km Segment of a Semiarid Stream. *Ecosystems*, *25*(2), 422–440. https://doi.org/10.1007/s10021-021-00661-5

Hosen, J. D., Aho, K. S., Appling, A. P., Creech, E. C., Fair, J. H., Hall Jr., R. O., Kyzivat, E. D., Lowenthal, R. S., Matt, S., Morrison, J., Saiers, J. E., Shanley, J. B., Weber, L. C., Yoon, B., & Raymond, P. A. (2019). Enhancement of primary production during drought in a temperate watershed is greater in larger rivers than headwater streams. *Limnology and Oceanography*, *64*(4), 1458–1472. https://doi.org/10.1002/lno.11127

Hotchkiss, E. R., Hall Jr, R. O., Sponseller, R. A., Butman, D., Klaminder, J., Laudon, H., Rosvall, M., & Karlsson, J. (2015). Sources of and processes controlling CO2 emissions change with the size of streams and rivers. *Nature Geoscience*, *8*(9), 696–699. https://doi.org/10.1038/ngeo2507

Hunt, R. J., Jardine, T. D., Hamilton, S. K., Bunn, S. E., & TROPICAL RIVERS and COASTAL KNOWLEDGE RESEARCH HUB. (2012). Temporal and spatial variation in ecosystem metabolism and food web carbon transfer in a wet-dry tropical river. *Freshwater Biology*, *57*(3), 435–450. https://doi.org/10.1111/j.1365-2427.2011.02708.x

Iannucci, F. M., Beneš, J., Medvedeff, A., & Bowden, W. B. (2021). Biogeochemical responses over 37 years to manipulation of phosphorus concentrations in an Arctic river: The Upper Kuparuk River Experiment. *Hydrological Processes*, *35*(3), e14075. https://doi.org/10.1002/hyp.14075

IPCC, 2014: Climate Change 2014: Synthesis Report. Contribution of Working Groups I, II and III to the Fifth Assessment Report of the Intergovernmental Panel on Climate Change [Core Writing Team, R.K. Pachauri and L.A. Meyer (eds.)]. IPCC, Geneva, Switzerland, 151 pp.

Jarvie, H. P., Macrae, M. L., Anderson, M., Celmer-Repin, D., Plach, J., & King, S. M. (2022). River metabolic fingerprints and regimes reveal ecosystem responses to enhanced wastewater treatment. *Journal of Environmental Quality*, *51*(5), 811–825. https://doi.org/10.1002/jeq2.20401

Jeffrey, S. W., & Humphrey, G. F. (1975). New spectrophotometric equations for determining chlorophylls a, b, c1 and c2 in higher plants, algae and natural phytoplankton. *Biochemie Und Physiologie Der Pflanzen*, *167*, 191–194. https://doi.org/10.1016/S0015-3796(17)30778-3

Johnston, S. E., Bogard, M. J., Rogers, J. A., Butman, D., Striegl, R. G., Dornblaser, M., & Spencer, R. G. M. (2019). Constraining dissolved organic matter sources and temporal variability in a model sub-Arctic lake. *Biogeochemistry*, *146*(3), 271–292. https://doi.org/10.1007/s10533-019-00619-9

Johnston, S. E., Gunawardana, P. V. S. L., Rood, S. B., & Bogard, M. J. (2022). Multidecadal Trends in Organic Carbon Flux Through a Grassland River Network Shaped by Human Controls and Climatic Cycles. *Geophysical Research Letters*, *49*(4), e2021GL096885. https://doi.org/10.1029/2021GL096885

Karlsson, J., Byström, P., Ask, J., Ask, P., Persson, L., & Jansson, M. (2009). Light limitation of nutrient-poor lake ecosystems. *Nature*, *460*, 506–509. https://doi.org/10.1038/nature08179

Kellerman, A. M., Dittmar, T., Kothawala, D. N., & Tranvik, L. J. (2014). Chemodiversity of dissolved organic matter in lakes driven by climate and hydrology. *Nature Communications*, *5*(1), Article 1. https://doi.org/10.1038/ncomms4804

Kritzberg, E., Cole, J., Pace, M., Graneli, W., & Bade, D. (2004). Autochthonous versus allochthonous carbon sources to bacteria: Results from whole-lake 13C addition experiments. *Limnology and Oceanography*, *49*. https://doi.org/10.4319/lo.2004.49.2.0588

Lapierre, J.-F., & del Giorgio, P. A. (2012). Geographical and environmental drivers of regional differences in the lake pCO2 versus DOC relationship across northern landscapes. *Journal of Geophysical Research: Biogeosciences*, *117*(G3). https://doi.org/10.1029/2012JG001945

Lapierre, J.-F., Guillemette, F., Berggren, M., & del Giorgio, P. A. (2013). Increases in terrestrially derived carbon stimulate organic carbon processing and CO2 emissions in boreal aquatic ecosystems. *Nature Communications*, *4*(1), Article 1. https://doi.org/10.1038/ncomms3972

Lauerwald, R., Laruelle, G. G., Hartmann, J., Ciais, P., & Regnier, P. A. G. (2015). Spatial patterns in CO2 evasion from the global river network. *Global Biogeochemical Cycles*, *29*(5), 534–554. https://doi.org/10.1002/2014GB004941

Little, J. L., Saffran, K. A., & Fent, L. (2003). Land Use and Water Quality Relationships in the Lower Little Bow River Watershed, Alberta, Canada. *Water Quality Research Journal*, *38*(4), 563–584. https://doi.org/10.2166/wqrj.2003.037

Maavara, T., Lauerwald, R., Regnier, P., & Van Cappellen, P. (2017). Global perturbation of organic carbon cycling by river damming. *Nature Communications*, *8*(1), 15347. https://doi.org/10.1038/ncomms15347

Maavara, T., Logozzo, L., Stubbins, A., Aho, K., Brinkerhoff, C., Hosen, J., & Raymond, P. (2021). Does Photomineralization of Dissolved Organics Matter in Temperate Rivers? *Journal of Geophysical Research: Biogeosciences*, *126*(7), e2021JG006402. https://doi.org/10.1029/2021JG006402

McGovern, M., Evenset, A., Borgå, K., De Wit, H. A., Braaten, H. F. V., Hessen, D. O., Schultze, S., Ruus, A., & Poste, A. (2019). Implications of Coastal Darkening for Contaminant Transport, Bioavailability, and Trophic Transfer in Northern Coastal Waters. *Environmental Science & Technology*, *53*(13), 7180–7182. https://doi.org/10.1021/acs.est.9b03093

Meyer, L., Brinkman, S., van Kesteren, L., Leprince-Ringuet, N., & van Boxmeer, F. (n.d.). *Technical Support Unit for the Synthesis Report*.

O'Donnell, B., & Hotchkiss, E. R. (2019). Coupling Concentration- and Process-Discharge Relationships Integrates Water Chemistry and Metabolism in Streams. *Water Resources Research*, *55*(12), 10179–10190. https://doi.org/10.1029/2019WR025025

Odum, H. T. (1956). Primary Production in Flowing Waters1. *Limnology and Oceanography*, *1*(2), 102–117. https://doi.org/10.4319/lo.1956.1.2.0102

Organic matter breakdown and ecosystem metabolism: Functional indicators for assessing river ecosystem health. (n.d.). https://doi.org/10.1899/07-121.1

Peterson, B. J., Hobbie, J. E., Hershey, A. E., Lock, M. A., Ford, T. E., Vestal, J. R., McKinley, V. L., Hullar, M. A. J., Miller, M. C., Ventullo, R. M., & Volk, G. S. (1985). Transformation of a Tundra River from Heterotrophy to Autotrophy by Addition of Phosphorus. *Science*, *229*(4720), 1383–1386. https://doi.org/10.1126/science.229.4720.1383

Ran, L., Lu, X. X., Yang, H., Li, L., Yu, R., Sun, H., & Han, J. (2015). CO2 outgassing from the Yellow River network and its implications for riverine carbon cycle. *Journal of Geophysical Research: Biogeosciences*, *120*(7), 1334–1347. https://doi.org/10.1002/2015JG002982

Raymond, P. A., Hartmann, J., Lauerwald, R., Sobek, S., McDonald, C., Hoover, M., Butman, D., Striegl, R., Mayorga, E., Humborg, C., Kortelainen, P., Dürr, H., Meybeck, M., Ciais, P., & Guth, P. (2013). Global carbon dioxide emissions from inland waters. *Nature*, *503*(7476), 355–359. https://doi.org/10.1038/nature12760

Raymond, P. A., Zappa, C. J., Butman, D., Bott, T. L., Potter, J., Mulholland, P., Laursen, A. E., McDowell, W. H., & Newbold, D. (2012). Scaling the gas transfer velocity and hydraulic geometry in streams and small rivers. *Limnology and Oceanography: Fluids and Environments*, *2*(1), 41–53. https://doi.org/10.1215/21573689-1597669

Reed, A. P., Stets, E. G., Murphy, S. F., & Mullins, E. A. (2021). Aquatic-Terrestrial Linkages Control Metabolism and Carbon Dynamics in a Mid-Sized, Urban Stream Influenced by Snowmelt. *Journal of Geophysical Research: Biogeosciences*, *126*(9), e2021JG006296. https://doi.org/10.1029/2021JG006296

Regnier, P., Friedlingstein, P., Ciais, P., Mackenzie, F. T., Gruber, N., Janssens, I. A., Laruelle, G. G., Lauerwald, R., Luyssaert, S., Andersson, A. J., Arndt, S., Arnosti, C., Borges, A. V., Dale, A. W., Gallego-Sala, A., Goddéris, Y., Goossens, N., Hartmann, J., Heinze, C., … Thullner, M. (2013).

Anthropogenic perturbation of the carbon fluxes from land to ocean. *Nature Geoscience*, *6*(8), 597–607. https://doi.org/10.1038/ngeo1830

Rocher-Ros, G., Sponseller, R. A., Lidberg, W., Mörth, C.-M., & Giesler, R. (2019). Landscape process domains drive patterns of CO2 evasion from river networks. *Limnology and Oceanography Letters*, *4*(4), 87–95. https://doi.org/10.1002/lol2.10108

Rocher-Ros, G., Stanley, E. H., Loken, L. C., Casson, N. J., Raymond, P. A., Liu, S., Amatulli, G., & Sponseller, R. A. (2023). Global methane emissions from rivers and streams. *Nature*, *621*(7979), Article 7979. https://doi.org/10.1038/s41586-023-06344-6

Rock, L., & Mayer, B. (2007). Isotope hydrology of the Oldman River basin, southern Alberta, Canada. *Hydrological Processes*, *21*(24), 3301–3315. https://doi.org/10.1002/hyp.6545

Rood, D. S. B., Samuelson, G. M., & Bigelow, S. G. (2005). *THE LITTLE BOW GETS BIGGER – ALBERTA'S NEWEST RIVER DAM*.

Rosemond, A. D., Benstead, J. P., Bumpers, P. M., Gulis, V., Kominoski, J. S., Manning, D. W. P., Suberkropp, K., & Wallace, J. B. (2015). Experimental nutrient additions accelerate terrestrial carbon loss from stream ecosystems. *Science*, *347*(6226), 1142–1145. https://doi.org/10.1126/science.aaa1958

Schindler, D. W. (2001). The cumulative effects of climate warming and other human stresses on Canadian freshwaters in the new millennium. *Canadian Journal of Fisheries and Aquatic Sciences*, *58*(1), 18–29. https://doi.org/10.1139/f00-179

Schindler, D. W., & Donahue, W. F. (2006). An impending water crisis in Canada's western prairie provinces. *Proceedings of the National Academy of Sciences*, *103*(19), 7210–7216. https://doi.org/10.1073/pnas.0601568103

Schlesinger, W. H., & Bernhardt, E. S. (2020). The Global Carbon and Oxygen Cycles. In *Biogeochemistry* (pp. 453–481). Elsevier. https://doi.org/10.1016/B978-0-12-814608-8.00011-6

Solano, V., Duvert, C., Birkel, C., Maher, D. T., García, E. A., & Hutley, L. B. (n.d.). Stream respiration exceeds CO2 evasion in a low-energy, oligotrophic tropical stream. *Limnology and Oceanography*, *n/a*(n/a). https://doi.org/10.1002/lno.12334

Song, C., Dodds, W. K., Rüegg, J., Argerich, A., Baker, C. L., Bowden, W. B., Douglas, M. M., Farrell, K. J., Flinn, M. B., Garcia, E. A., Helton, A. M., Harms, T. K., Jia, S., Jones, J. B., Koenig, L. E., Kominoski, J. S., McDowell, W. H., McMaster, D., Parker, S. P., … Ballantyne, F. (2018). Continental-scale decrease in net primary productivity in streams due to climate warming. *Nature Geoscience*, *11*(6), 415–420. https://doi.org/10.1038/s41561-018-0125-5

Sosiak, A. (n.d.). *Analysis of Water Quality Sampling of Twin Valley Reservoir, Clear Lake and Tributaries, 1999-2010*.

Soued, C., Del Giorgio, P. A., & Maranger, R. (2016). Nitrous oxide sinks and emissions in boreal aquatic networks in Québec. *Nature Geoscience*, *9*(2), 116–120. https://doi.org/10.1038/ngeo2611

Soued, C., Giorgio, P., & Maranger, R. (2015). Nitrous oxide sinks and emissions in boreal aquatic networks in Quebec, Canada. *Nature Geoscience*, *9*. https://doi.org/10.1038/ngeo2611

Stets, E. G., Butman, D., McDonald, C. P., Stackpoole, S. M., DeGrandpre, M. D., & Striegl, R. G. (2017). Carbonate buffering and metabolic controls on carbon dioxide in rivers. *Global Biogeochemical Cycles*, *31*(4), 663–677. https://doi.org/10.1002/2016GB005578

Talbot, C. J., Bennett, E. M., Cassell, K., Hanes, D. M., Minor, E. C., Paerl, H., Raymond, P. A., Vargas, R., Vidon, P. G., Wollheim, W., & Xenopoulos, M. A. (2018). The impact of flooding on aquatic ecosystem services. *Biogeochemistry*, *141*(3), 439–461. https://doi.org/10.1007/s10533-018-0449-7

Teyssier, D., Fossé, D., Gerin, M., Pety, J., Abergel, A., & Roueff, E. (2004). Carbon budget and carbon chemistry in Photon Dominated Regions. *Astronomy & Astrophysics*, *417*(1), 135–149. https://doi.org/10.1051/0004-6361:20034534

Tranvik, L. J., Downing, J. A., Cotner, J. B., Loiselle, S. A., Striegl, R. G., Ballatore, T. J., Dillon, P., Finlay, K., Fortino, K., Knoll, L. B., Kortelainen, P. L., Kutser, T., Larsen, Soren., Laurion, I., Leech, D. M., McCallister, S. L., McKnight, D. M., Melack, J. M., Overholt, E., … Weyhenmeyer, G. A. (2009). Lakes and reservoirs as regulators of carbon cycling and climate. *Limnology and Oceanography*, *54*(6part2), 2298–2314. https://doi.org/10.4319/lo.2009.54.6_part_2.2298

Uehlinger, U. (2006). Annual cycle and inter-annual variability of gross primary production and ecosystem respiration in a floodprone river during a 15-year period. *Freshwater Biology*, *51*(5), 938–950. https://doi.org/10.1111/j.1365-2427.2006.01551.x

Ulseth, A. J., Hall, R. O., Boix Canadell, M., Madinger, H. L., Niayifar, A., & Battin, T. J. (2019). Distinct air–water gas exchange regimes in low- and high-energy streams. *Nature Geoscience*, *12*(4), 259–263. https://doi.org/10.1038/s41561-019-0324-8

Ulseth, A. J., & Hall, R. O. J. (2015). Dam tailwaters compound the effects of reservoirs on the longitudinal transport of organic carbon in an arid river. *Biogeosciences*, *12*(14), 4345–4359. https://doi.org/10.5194/bg-12-4345-2015

Vonk, J. E., Tank, S. E., Mann, P. J., Spencer, R. G. M., Treat, C. C., Striegl, R. G., Abbott, B. W., & Wickland, K. P. (2015). Biodegradability of dissolved organic carbon in permafrost soils and aquatic systems: A meta-analysis. *Biogeosciences*, *12*(23), 6915–6930. https://doi.org/10.5194/bg-12-6915-2015

Wang, J., Wang, X., Liu, T., Yuan, X., Chen, H., He, Y., Wu, S., Yuan, Z., Li, H., Que, Z., Yu, L., & Zhang, Y. (2021). pCO2 and CO2 evasion from two small suburban rivers: Implications of the watershed urbanization process. *Science of The Total Environment*, *788*, 147787. https://doi.org/10.1016/j.scitotenv.2021.147787

Wanninkhof, R. (1992). Relationship between wind speed and gas exchange over the ocean. *Journal of Geophysical Research*, *97*(C5), 7373. https://doi.org/10.1029/92JC00188

Webb, J. R., Santos, I. R., Maher, D. T., & Finlay, K. (2019). The Importance of Aquatic Carbon Fluxes in Net Ecosystem Carbon Budgets: A Catchment-Scale Review. *Ecosystems*, *22*(3), 508–527. https://doi.org/10.1007/s10021-018-0284-7

Weiss, R. F. (1974). Carbon dioxide in water and seawater: The solubility of a non-ideal gas. *Marine Chemistry*, *2*(3), 203–215. https://doi.org/10.1016/0304-4203(74)90015-2

White, J. S. (1999). Restoration of a Canadian Prairie Wetland with Agricultural and Municipal Wastewater. *Environmental Management*, *24*(1), 25–37. https://doi.org/10.1007/s002679900212

Xenopoulos, M. A., Barnes, R. T., Boodoo, K. S., Butman, D., Catalán, N., D'Amario, S. C., Fasching, C., Kothawala, D. N., Pisani, O., Solomon, C. T., Spencer, R. G. M., Williams, C. J., & Wilson, H. F. (2021). How humans alter dissolved organic matter composition in freshwater: Relevance for the Earth's biogeochemistry. *Biogeochemistry*, *154*(2), 323–348. https://doi.org/10.1007/s10533-021-00753-3

Yan, X., Thieu, V., Wu, S., & Garnier, J. (2022). Reservoirs change pCO2 and water quality of downstream rivers: Evidence from three reservoirs in the Seine Basin. *Water Research*, *213*, 118158. https://doi.org/10.1016/j.watres.2022.118158

Young, R. G., Matthaei, C. D., & Townsend, C. R. (2008a). Organic matter breakdown and ecosystem metabolism: Functional indicators for assessing river ecosystem health. *Journal of the North American Benthological Society*, *27*(3), 605–625. https://doi.org/10.1899/07-121.1

Young, R. G., Matthaei, C. D., & Townsend, C. R. (2008b). Organic matter breakdown and ecosystem metabolism: Functional indicators for assessing river ecosystem health. *Journal of the North American Benthological Society*, *27*(3), 605–625. https://doi.org/10.1899/07-121.1

Zhou, X., Johnston, S. E., & Bogard, M. J. (2023). Organic matter cycling in a model restored wetland receiving complex effluent. *Biogeochemistry*, *162*(2), 237–255. https://doi.org/10.1007/s10533-022-01002-x

Zhu, D., Ryan, M. C., & Gao, H. (2019). The role of water and mass balances in treatment assessment of a flooded natural wetland receiving wastewater effluent (Frank Lake, Alberta, Canada). *Ecological Engineering*, *137*, 34–45. https://doi.org/10.1016/j.ecoleng.2019.01.010

APPENDIX- A

Figure A1. LBCAN sampling site

Figure A2. LBUP sampling site

Figure A3. LB533 sampling site

Figure A4. MCR sampling site

Figure A5. MCRDIV sampling site

Figure A6. TVRD sampling site

Figure A7. LBCAR sampling site

APPENDIX B

Table B1. Location of routine sampling sites within the ULB watershed

Site	Latitude	Longitude
LBCAN	50.55016	-113.85699
LBUP	50.47814	-113.66809
LB533	50.35317	-113.54404
MCR	50.25171	-113.55399
MCRDIV	50.23703	-113.47765
TVRD	50.22431	-113.39572
LBCAR	50.13412	-113.13988

APPENDIX C

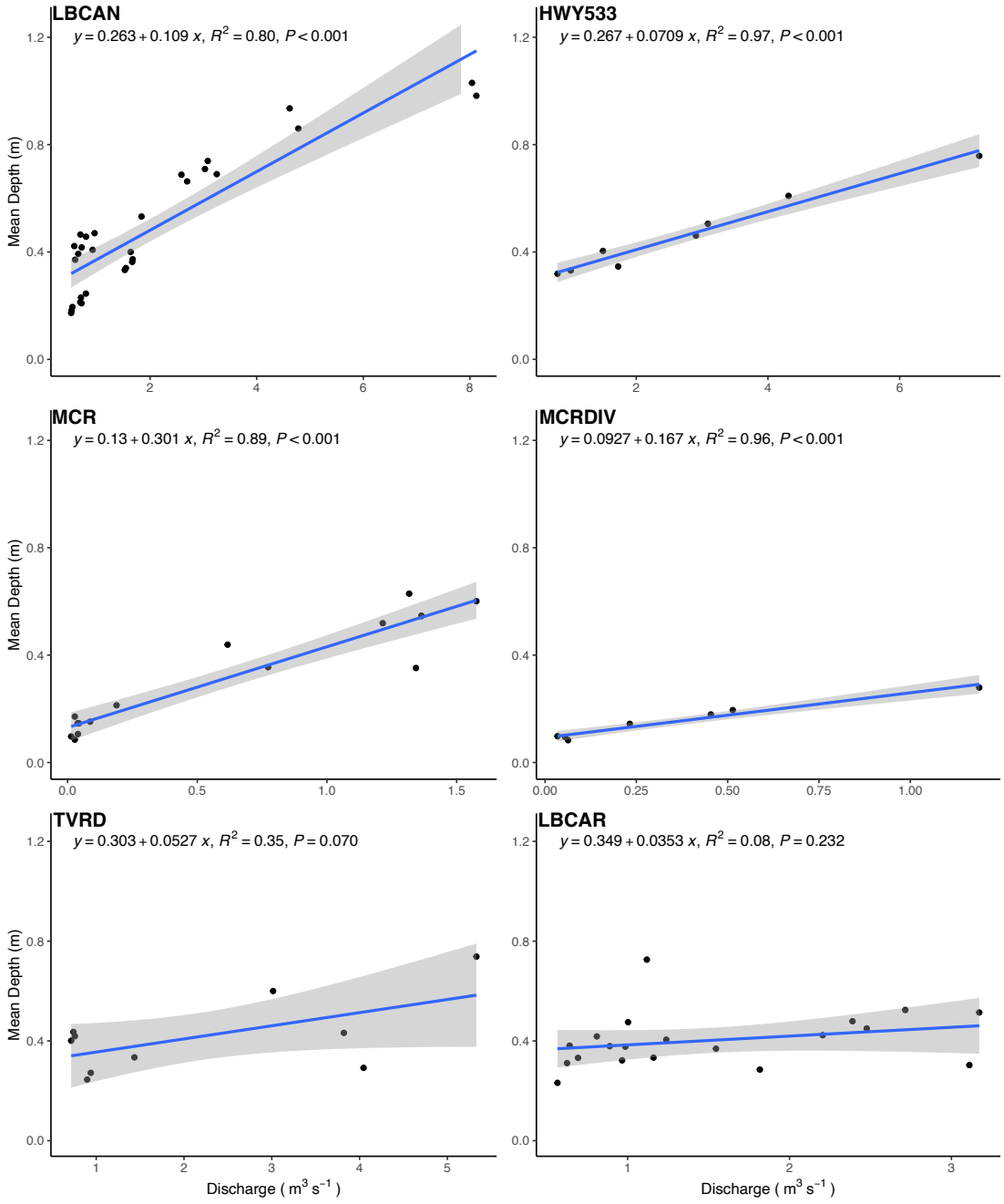

Figure C1. Site-specific relationships of mean depth as a function of discharge.

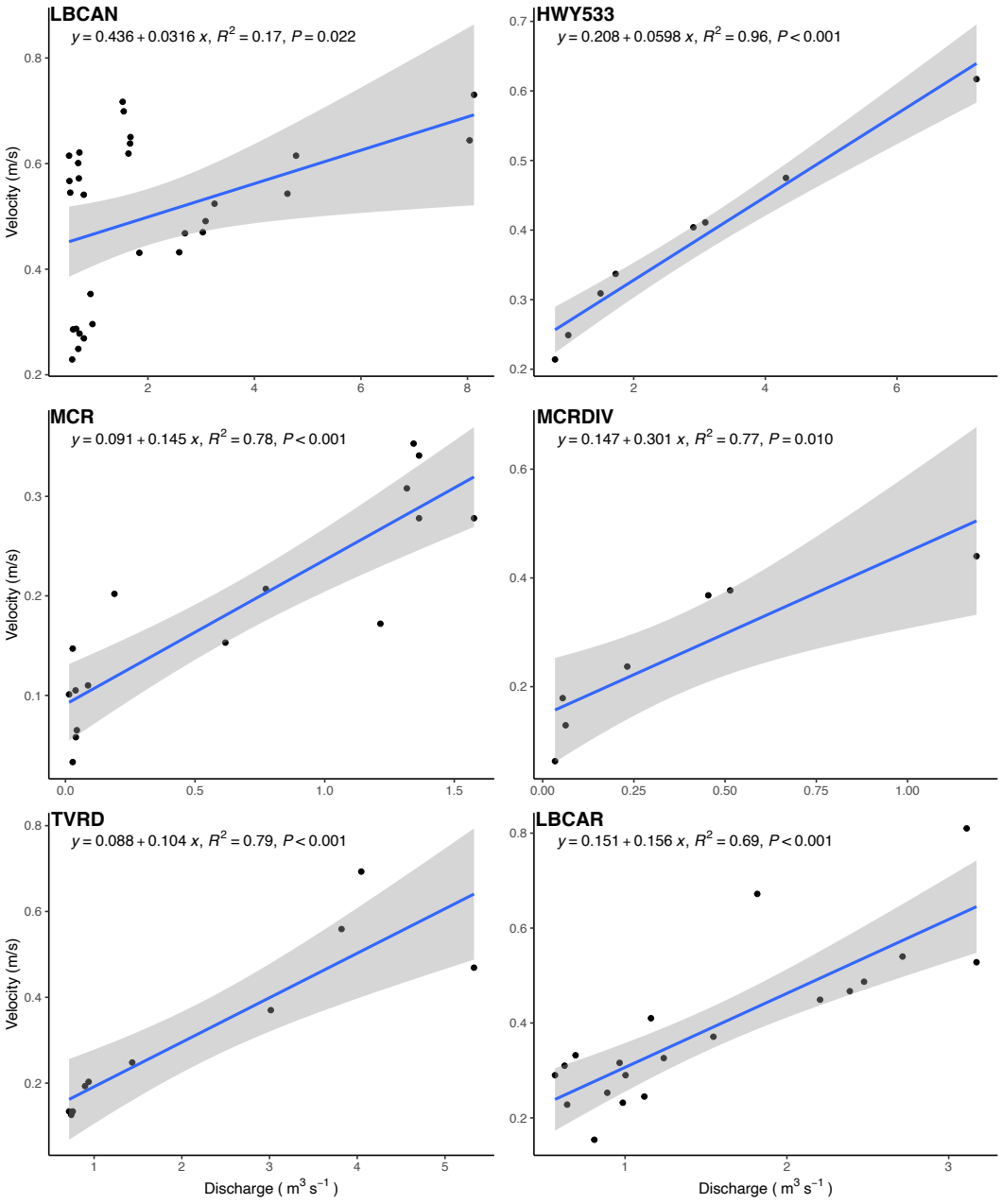

Figure C2. Site-specific relationships of river velocity as a function of discharge.

APPENDIX D

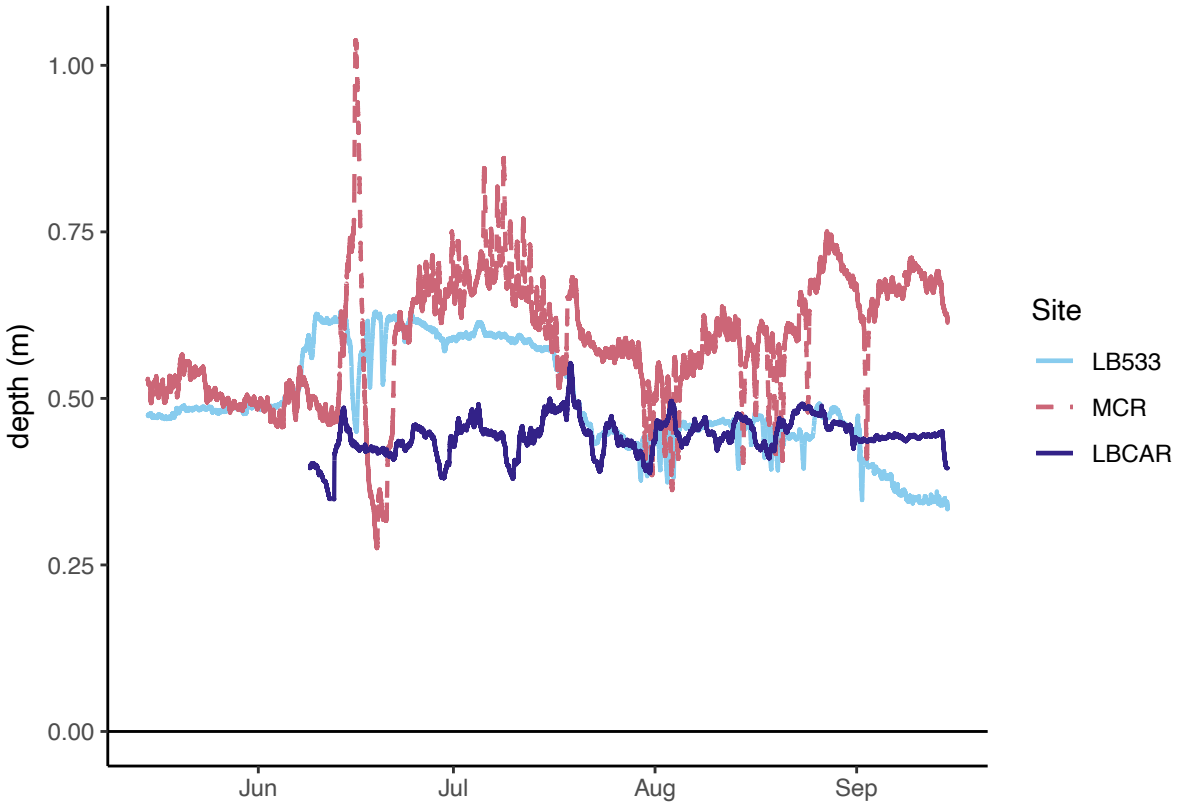

Figure D1. Mean depth (m) measurements for three modelled sites.

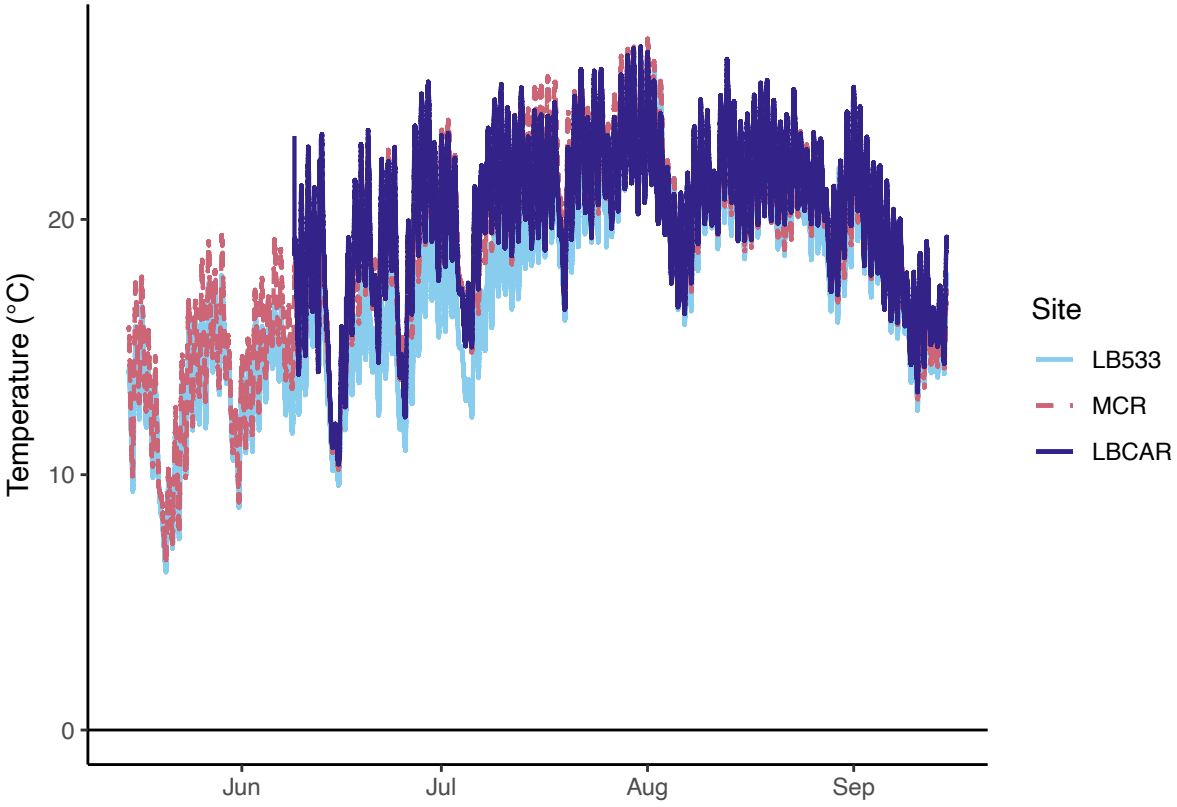

Figure D2. High frequency temperature measurements for three modelled sites.